Available online at www.sciencedirect.com
SCIENCE DIRECT
Journal of Sound and Vibration 294 (2006) 503–528
JOURNAL OF SOUND AND VIBRATION
www.elsevier.com/locate/jsvi

Influence of harmonically varying normal load on steady-state behavior of a 2dof torsional system with dry friction

Chengwu Duan, Rajendra Singh*

Acoustics and Dynamics Laboratory, Department of Mechanical Engineering, The Center for Automotive Research, The Ohio State University, Columbus, OH 43202, USA

Received 4 November 2004; accepted 22 November 2005
Available online 23 February 2006

Abstract

A nonlinear dry friction problem with harmonically varying normal load is formulated, in the context of a two-degree of freedom torsional system, since virtually all of the prior literature focuses on the topic of time-invariant normal load. First, pure stick, pure slip and stick–slip motions are computationally and analytically determined when excited by a sinusoidal torque, in the presence of harmonically varying saturation torque; mean terms are included in both. These analyses yield both transient and steady-state time histories under various conditions. Second, the effects of time-varying normal load on steady-state responses have been investigated and nonlinear spectral maps (including super-harmonics) are developed. Results show that the actuation system parameters could affect steady-state stick–slip motions in different ways over the lower and higher frequency regimes, as a result of time-delay in slip motions with respect to the torque excitation. In particular, the negative slope characteristics in the friction law exaggerate the stick–slip vibration problems, and it is the major cause of bifurcations and quasi-periodic or chaotic motions. Around the super-harmonic peak frequencies, the nonlinear system tends to lose stability as abrupt jumps in the spectral maps take place. An equivalent viscous damping model is considered to analytically investigate the instability mechanism. Further, the periodicity of the system response under harmonically varying actuation is conceptually by employing the harmonic balance method. Finally, steady-state behavior is examined for the nonlinear, time-varying dry friction problem.

1. Introduction

Dry friction elements are encountered in many mechanical and structural systems, under a variety of operational conditions [1–10]. First, consider the classical friction damper example of Fig. 1(a) where a single-degree-of-freedom (sdof) torsional system is shown. Assuming a time-invariant normal load N, the equation of motion is $I\ddot{\theta} + T_c(\theta, \dot{\theta}) + T_f(N, \dot{\theta}) = T_e(t)$ where $T_c(\theta, \dot{\theta})$ is the constraint torque, $T_e(t)$ is the externally applied torque excitation, I is the inertia, θ is the angular displacement and T_f is the friction torque given time-invariant N; one could employ one of the several $T_f(\dot{\theta})$ relationships [3,6,8–10]. Indeed, there is a

Abbreviations: LHS, left-hand side; max, maximum value; NLTV, nonlinear time-varying; RHS, right-hand side; sdof, single-degree-of-freedom system; TCC, torque converter clutch; 2dof, 2-degree-of-freedom system

*Corresponding author. Tel.: +1 614 292 9044; fax +1 614 292 3163.
E-mail address: singh.3@osu.edu (R. Singh).

0022-460X/$ - see front matter © 2006 Elsevier Ltd. All rights reserved.
doi:10.1016/j.jsv.2006.01.001

Nomenclature

A	area of actuation pressure
C	torsional viscous damping coefficient
I	torsional inertia
K	torsional stiffness
N	normal force
P	pressure
R	moment arm
t	time
T	torque
α	exponentially decaying factor
δ	relative angular displacement
ω	angular frequency
ψ	phase lag
θ	absolute angular displacement
σ	conditioning factor
Ω	angular speed
ζ	various damping ratio
μ	friction coefficient

Subscripts

1, 2, 3	inertial element indices
c	constraint
d	damped
e	engine
f	friction
k	kinetic
m	mean
max	maximum
n	natural frequency
p	fluctuating component or perturbation
s	static or saturation
ss	steady state
t	transmission

Superscripts

–	normalized value
.	first derivative with respect to time
..	second derivative with respect to time

Operators

$\|\ \|$	absolute value
$< >_t$	time-average operator

substantial body of literature on time-invariant friction torque or force, especially when the saturation forces or torques are small [1–8]. Second, assume that N varies with time, say intentionally through an actively controlled actuation mechanism that applies time-varying pressure $P(t)$ on an area A. Thus the nonlinear, time-varying (NLTV) friction torque $T_f(N(t), \dot{\theta})$ is given by $\mu N(t)R = \mu P(t)AR$, where R is a moment arm and μ is the coefficient of friction. Of course, one may find yet physical processes where the contact loads may change periodically anyway, such as in gear pairs [11,12]. To the best of our knowledge, no prior researcher has addressed the harmonically varying nonlinear friction force or torque issue, with the exception of sliding friction in gears [11,12].

2. Problem formulation

2.1. Physical system

In this article, we investigate the effect of harmonically varying normal load $N(t)$ on the dynamics of a two-degree-of-freedom (2dof) torsional system with nonlinear dry friction path. Example systems include the slipping torque converter clutch (TCC) in an automotive driveline system as schematically illustrated in Fig. 1(b). Other applications may include smart clutch [13] and dual clutch transmission [14,15] concepts. Unlike a pure dry friction damper (such as the one in Fig. 1(a)), the dry friction element in Fig. 1(b) functions as a key power transmission path. For example, in a vehicle with automatic transmission, the fuel economy can be improved by applying a slipping TCC to avoid the power loss within the fluid torque converter [16,17]. As shown in Fig. 1(b), the nonlinear friction torque T_{sf} transmitted within the TCC is applied by a hydraulic actuation pressure $P(t)$, which is controlled by a pulse-width modulated solenoid valve [18]. Accordingly, a time-varying normal load is created assuming a fixed pressure area for a given physical system, i.e. $N(t) = P(t)A$. By controlling P or N, a target slip speed $(\Omega_e - \Omega_t)$ is achieved, ensuring a best compromise

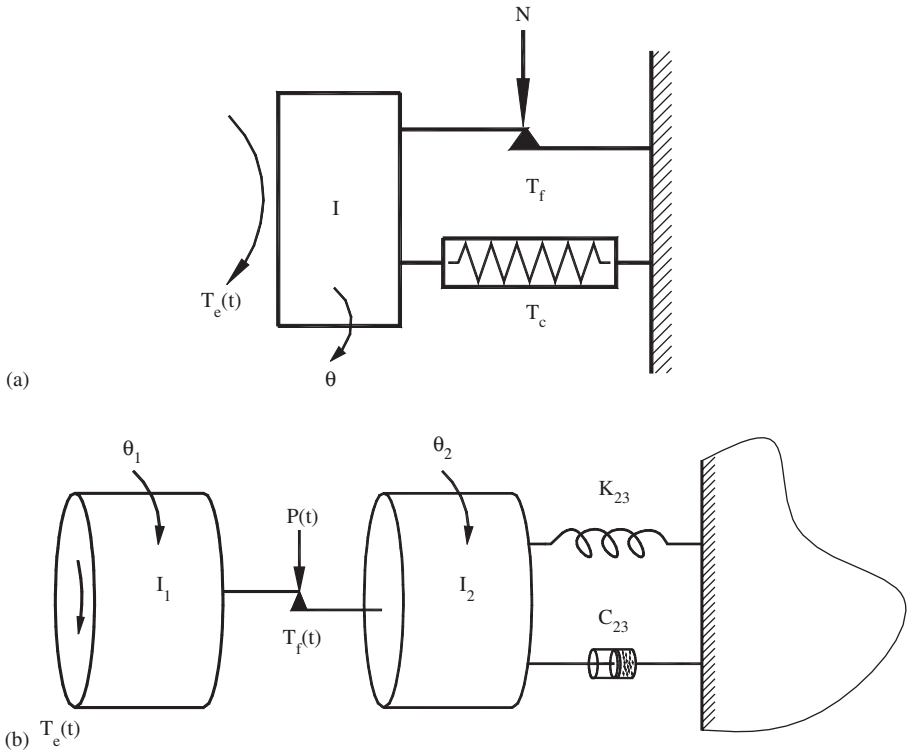

Fig. 1. Torsional systems with dry friction element: (a) classical sdof dry friction damper system; (b) example case of this article: 2dof driveline system with time-varying normal load in the dry friction path.

between the fuel efficiency and ride quality [18,19]. Several researchers have studied the effect of the feedback control systems and hydraulic actuation system dynamics [18,20]. However, the essential dry friction nonlinearity has been either ignored or linearized around the operating point assuming small motions.

Recently, Duan and Singh investigated system dynamics of a torsional system with a dry friction controlled path [21,22]. Significant stick–slip motions are found under harmonic torque excitation. Nonlinear frequency response characteristics have been studied using analytical or semi-analytical methods. However, a constant N was assumed in the previous studies. In this article, we assume the normal load N to be sinusoidal with a mean (dc) term, as a result of the oscillations within the hydraulic control circuit [18]. We also consider the possibility of a negative slope in the friction characteristics (the Stribeck effect of the lining material). Both of these effects could induce quasi-periodic or chaotic responses and consequently pose difficulty for the system control and introduce objectionable noise and vibration problems to the vehicle systems.

2.2. Governing equations of 2dof torsional system

The vehicle driveline system can be represented by a simplified 2dof torsional model as in Fig. 1(b). Here, I_1 represents the combined torsional inertia of flywheel, I_2 is the inertia of friction shoe and pressure plate and the wheel and vehicle sub-system I_3 is considered as ground. The governing equations are

$$I_1\ddot{\theta}_1 + T_f(\dot{\theta}_1 - \dot{\theta}_2,\ t) = T_e(t) = T_m + T_p\ \sin(\omega t), \tag{1a}$$

$$I_2\ddot{\theta}_2 + C_{23}\dot{\theta}_2 + K_{23}\theta_2 = T_f(\dot{\theta}_1 - \dot{\theta}_2,\ t). \tag{1b}$$

Here, θ_1 and θ_2 are absolute angular displacements; C_{23} and K_{23} are the lumped viscous damping and stiffness associated with the automotive driveline. Further, we reformulate the equations in terms of relative motions

where $\delta_1 = \theta_1 - \theta_2$ and$\delta_2 = \theta_2$:

$$I_1\ddot{\delta}_1 - \frac{I_1}{I_2}C_{23}\dot{\delta}_2 - \frac{I_1}{I_2}K_{23}\delta_2 + \left(1.0 + \frac{I_1}{I_2}\right)T_f(\dot{\delta}_1,\ t) = T_m + T_p\ \sin(\omega t), \tag{2a}$$

$$I_2\ddot{\delta}_2 + C_{23}\dot{\delta}_2 + K_{23}\delta_2 = T_f(\dot{\delta}_1,\ t). \tag{2b}$$

The engine torque excitation $T_e(t)$ is composed of mean $T_m = <T_e>_t$ and pulsating $T_p(t)$ components, where $<\ >_t$ is the time-average operator. Using the Fourier series expansion, express it as $T_e(t) = T_m + \sum_n T_{pn}\sin(\omega_{pn}t + \phi_{pn})$, where n is the harmonic order of the firing torque sequence, $\omega_{pn} = (N_e/2)n\Omega_e$, N_e is the number of engine cylinders [23], T_{pn} is the amplitude for the nth harmonic and ϕ_n is the associated phase lag. In this study, only the dominant harmonic component ($\omega_{p1} = \omega$) is considered for the sake of simplicity, i.e. $T_e(t) = T_m + T_p\ \sin(\omega t)$.

2.3. Friction torque formulation

The nonlinear friction torque $T_f(\dot{\delta}_1, t)$ is carried by the clutch and then it acts as an equivalent torque excitation to the downstream system. In a realistic automotive system, a pulse-width modulated solenoid valve would generate a time-varying P by changing the command value or duty ratio [18]. That results in a nonlinear time-varying (NLTV) friction torque formulation, $T_f(\dot{\delta}, t) = \mu(\dot{\delta})N(t)R$. Note that R is assumed to be time invariant. Assume $N(t)$ as a sinusoidal signal with mean pressure N_m, amplitude N_p and the actuation load frequency ω_f:

$$N(t) = N_m + N_p\ \sin(\omega_f t + \psi). \tag{3}$$

Here, ψ is the phase lag between the actuation load (pressure) and $T_e(t)$. Further, $N(t)$ is assumed to be positive-definite to ensure that no separation occurs across the frictional interface, i.e. $N_p/N_m \in [0, 1)$. We employ the following friction formulation $\mu(\dot{\delta}_1)$ to examine the phenomenological dynamic behavior [9]:

$$\mu(\dot{\delta}_1) = \begin{cases} \left[\mu_k + (\mu_s - \mu_k)\mathrm{e}^{-\alpha|\dot{\delta}_1|}\right]\mathrm{sgn}(\dot{\delta}_1), & |\dot{\delta}_1| > 0, \\ [0 \sim \mu_s], & \dot{\delta}_1 = 0. \end{cases} \tag{4}$$

Here, α is a positive constant that controls the gradient of μ with respect to $\dot{\delta}_1$. In our study, $\alpha = 2$ is chosen for the sake of illustration. In addition, a multi-valued regime exists at $\dot{\delta}_1 = 0$. To facilitate parametric studies, we incorporate some parameters such as μ_k and R into $N(t)$ to yield the following NLTV friction torque:

$$T_f(\dot{\delta}, t) = \bar{\mu}(\dot{\delta}_1)T_s(t), \quad T_s(t) = \mu_k N(t)R = T_{sm} + T_{sp}\ \sin(\omega_f t + \psi). \tag{5a,b}$$

Here, $\bar{\mu}(\dot{\delta}_1)$ is a normalized friction coefficient with respect to μ_k:

$$\bar{\mu}(\dot{\delta}_1) = \begin{cases} \left[1.0 + \left(\frac{\mu_s}{\mu_k} - 1.0\right)\mathrm{e}^{-\alpha|\dot{\delta}_1|}\right]\mathrm{sgn}(\dot{\delta}_1), & |\dot{\delta}_1| > 0, \\ \left[0 \sim \frac{\mu_s}{\mu_k}\right], & \dot{\delta}_1 = 0. \end{cases} \tag{6}$$

2.4. Objectives

The first objective is to analytically determine the nature of steady-state responses of the torsional system under harmonically varying dry friction. Analytical solutions under assumed motion conditions will also be developed to understand the dynamic behavior. The second objective is to analytically and numerically examine the steady-state responses under the effect of $N(t)$ and compare with the time-invariant case with nonlinear dry friction. Both periodic and chaotic responses will be identified via results in time and frequency domains. Further, bifurcation diagram and Poincare sections will be constructed by cascading the steady-state time-domain responses. Interaction between the clutch actuation parameters such as ψ, ω_f and T_{sp}, and the negative slope friction characteristics will be examined.

3. Computational methodology

For a piece-wise linear or nonlinear element such as dry friction, two numerical schemes, namely the discontinuous and continuous solutions, can be employed. The first one finds the solutions for different states and then assembles them [3,8,21]. This method can give an "exact" solution of the non-analytical system but enormous time is often required in the iterative matching process. Recently, Leine successfully employed Hénon's scheme but it is not convenient for a multi-degree-of-freedom system [6]. The second method employs a stiff differential equation solver but one must first condition the discontinuous nonlinearity. Typical conditioning functions include arctangent, hyper-tangent and the like [6,21,25]. This method is computationally efficient but an artificial uncertainty is introduced by the smoothening factor σ. Based on Duan and Singh's study [21], the user must exercise caution and use the discontinuous solution as a benchmark. Several researchers have recently used the harmonic balance method to study the nonlinear systems. For example, Blankenship and Kahraman developed a harmonic balance method to study the geared system under parametric excitation [26]. However, their method cannot be conveniently implemented especially when many harmonics must be included in the expansion. More recently, Kim et al. [27] and Duan and Singh [22] have proposed refined multi-term harmonic balance but both formulations are not suitable for a system with time-varying parameters because the procedure that converts the residue from time domain to frequency domain by factoring out the discrete Fourier transform matrix is no longer feasible. Further, analytical methods such as multi-term harmonic balance always look for periodic steady-state solutions. Quasi-period or chaotic responses that are of particular importance from the vehicle performance standpoint cannot be obtained.

To efficiently obtain a complete map of the system behavior including both periodic and aperiodic responses, an explicit Runge–Kutta 4th(5th) order numerical integration routine with adaptive step size control (designate as RK45) due to Dormand and Prince is employed [28]. This numerical solution will be validated, by comparing our predictions with those obtained by a popular ordinary differential solver *Xppaut* [24,30]. To facilitate the direct numerical integration, the discontinuous friction law of Eq. (6) is conditioned employing a hyper-tangent function with a smoothening factor $\sigma = 50$:

$$\bar{\mu}(\dot{\delta}_1) = \left[1.0 + \left(\frac{\mu_s}{\mu_k} - 1.0\right) e^{-\alpha|\dot{\delta}_1|}\right] \tanh(\sigma\dot{\delta}_1). \tag{7}$$

Fig. 2 illustrates the typical steady-state stick–slip behavior. First note that our numerical solution RK45 matches quite well with the discontinuous method of Ref. [31] and Gear's method (Gear) that is recommended by the *Xppaut* software for stiff nonlinear problems [24,30]. Differences are seen when the classical Runge–Kutta fourth order routine (RK4) of the *Xppaut* software is selected, possibly due to the numerical stability problem and as a result of the stiff nature computational problem at hand.

4. Nature of steady-state responses based on approximate analytical solution

For the physical system of Fig. 1(b), three kinds of steady-state responses across the frictional interface are possible following the initial transients: pure stick, pure slip and stick–slip. While the stick–slip is essentially controlled by the strong nonlinearity of dry friction element, pure stick or pure slip can be determined ahead of a numerical simulation by using simplified analytical solutions. For example, Duan and Singh [22] have proposed a procedure to determine the pure stick response regime for a time-invariant dry friction torque; this still holds for a time-varying dry friction formulation. Assume the pure stick motion ($\dot{\delta}_1 = 0$) that would consolidate I_1 and I_2 into a single inertial body. The nonlinear system of Fig. 1(b) would now behave as a linear system. The internal friction force T_{fi} across the interface is determined by $(T_e(t) - I_1\ddot{\theta}_1)$, where $\ddot{\theta}_1 = \ddot{\delta}_2$ under the condition $\dot{\delta}_1 = 0$:

$$\delta_2 = \frac{T_m}{K_{23}} + \frac{T_p}{\sqrt{(K_{23} - (I_1 + I_2)\omega^2)^2 + (C_{23}\omega)^2}} \sin(\omega t + \varphi), \tag{8a}$$

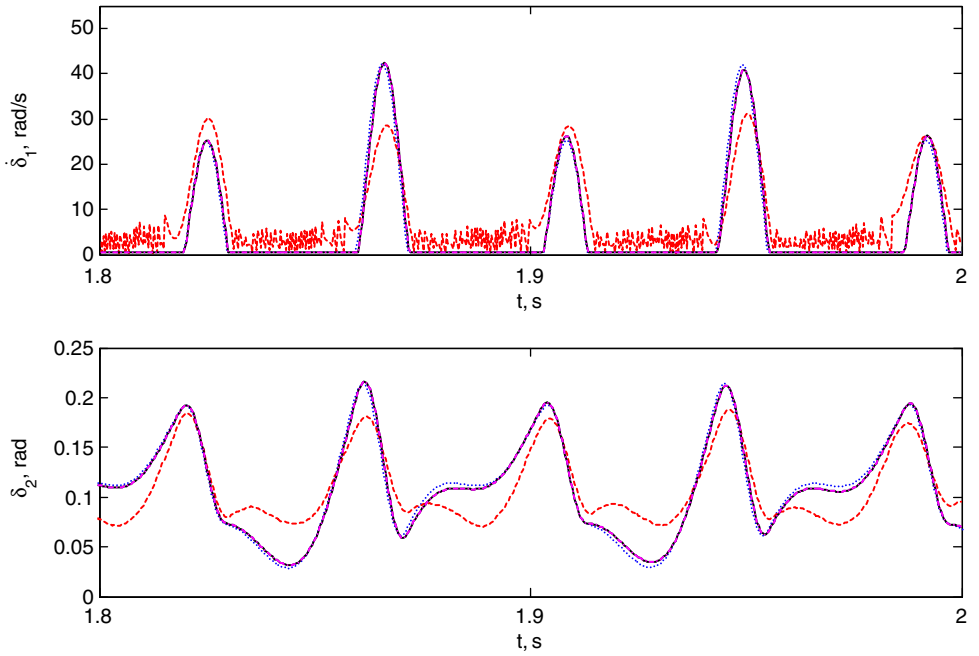

Fig. 2. Typical steady-state response for the 2dof torsional system given $\omega = 150$ rad/s, $T_m = 300$, $T_p = 250$, $T_{sm} = 500$, $T_{sp} = 0.2\ T_{sm}$, $\omega_f = \omega$, $\psi = 0$, $\mu_k = 0.8\mu_k$ and $\Omega_e = 150$ rad/s: ___ , RK45, … , gear, _ _ _ , RK4 methods, _·_, discontinuous solution.

$$\varphi = -\tan^{-1}\frac{C_{23}\omega}{K_{23} - (I_1 + I_2)\omega^2}. \tag{8b}$$

Thus,

$$T_{fi}(t) = T_m + T_p\ \sin(\omega t) + \frac{\omega^2 T_p}{\sqrt{(K_{23} - (I_1 + I_2)\omega^2)^2}}\sin(\omega t + \varphi). \tag{9}$$

When the internal friction torque is asymptotically less than the time-varying dry friction, pure stick motion is satisfied:

$$T_{fi}(t) \leqslant \mu_s N(t) R \quad \forall t \in [0, \infty). \tag{10}$$

Thus, we define a difference variable $\Delta(t) = T_{fi}(t) - \mu_s N(t) R$ and given its periodicity, the following criterion is defined to satisfy the pure stick condition:

$$\Delta(t) \leqslant 0 \quad \forall t \in [0,\ P_{\text{period}}), \quad P_{\text{period}} = \frac{2\pi}{\omega}. \tag{11a,b}$$

As noted, when the amplitudes of excitation and friction torques are fixed, the lower and higher transition frequencies from pure stick to stick–slip can be determined via upward and downward frequency sweeps, respectively [22]. However, it should be pointed out that this process is based on the piece-wise nonlinear friction law (6). In contrast, when that smoothened friction law (7) is used, the following two effects are brought into the system dynamics. First, the assumption of only pure stick motions may not be valid. Second, the maximum friction coefficient or torque decreases with μ_k given the same μ_s value as a result of the smoothening process as shown in Fig. 3. Thus, the resulting "transition" frequency would be affected by the value of μ_k, as explored in a subsequent section.

Further, pure slip type steady-state motions are possible as reported by Duan and Singh [29]. As a result of the speed difference between I_1 and I_2 during the initial engagement, a pure slip transient would exist [29]. If we were to assume pure positive slip motion ($\dot{\delta}_1 > 0$) and that $\mu_k = \mu_s$ since the negative gradient would

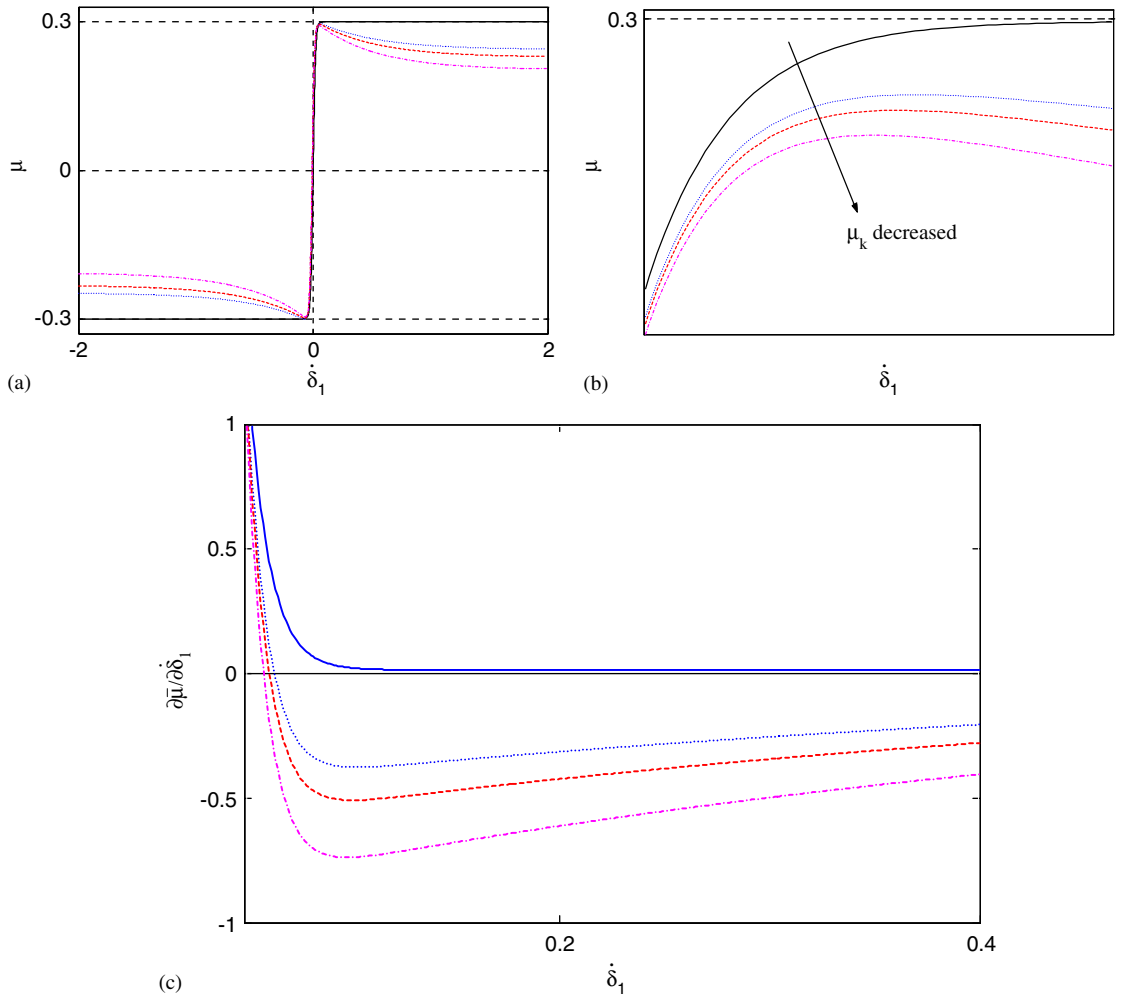

Fig. 3. Effect of smoothening on the friction coefficient vs. velocity relations: (a) smoothened friction law; (b) zoomed part; (c) calculated $\partial\bar{\mu}/\partial\dot{\delta}_1$. Key: ___ , $\mu_k = \mu_s$; … , $\mu_k = 0.8\mu_s$; _ _ _, $\mu_k = 0.75\mu_s$, _·_, $\mu_k = 0.677\mu_s$.

dominate only when $\dot{\delta}_1$ approaches zero, Eqs. (2a) and (2b) can be approximated as

$$I_1\ddot{\delta}_1 - \frac{I_1}{I_2}C_{23}\dot{\delta}_2 - \frac{I_1}{I_2}K_{23}\delta_2 + \left(1.0 + \frac{I_1}{I_2}\right)(T_{sm} + T_{sp}\,\sin(\omega_f t + \psi)) = T_m + T_p\,\sin(\omega t), \tag{12a}$$

$$I_2\ddot{\delta}_2 + C_{23}\dot{\delta}_2 + K_{23}\delta_2 = T_{sm} + T_{sp}\,\sin(\omega_f t + \psi). \tag{12b}$$

Together with the following initial conditions as assumed according to the physical system behavior:

$$\delta_1(0) = 0, \quad \dot{\delta}_1(0) = \Omega_e, \quad \delta_2(0) = 0, \quad \dot{\delta}_2(0) = 0. \tag{13a–d}$$

Through mathematical manipulation, Duan and Singh [29] obtain the following functional form where the coefficients a_0, a_1, a_{21}, a_{22} and a_3 are determined by Eq. (13):

$$\dot{\delta}_1(t) = a_0 + a_1 t + \left\{ \begin{array}{c} a_{21}\,\sin(\omega t + \varphi_{21}) \\ +a_{22}\,\sin(\omega_f t + \varphi_{22}) \end{array} \right\} + a_3 e^{-\zeta\omega_n t}\,\sin(\omega_d t + \varphi_3). \tag{14}$$

Table 1
Parameters and excitation amplitude used for simulating the driveline system of Fig. 1b

Parameters and excitation	Value(s)
Torsional inertias (kg m^2)	$I_1 = 0.20$; $I_2 = 0.02$
Torsional viscous damping (Nm rad/s)	$C_{23} = 0.6$
Torsional stiffness (Nm/rad)	$K_{23} = 3000$
Engine torque: mean and excitation amplitude (Nm)	$T_m = 300$; $T_p = 250$
Static (μ_s) and kinetic (μ_k) friction coefficients	$\mu_s = 0.3$; $\mu_k = 0.15$–0.30
Actuation pressure area (m^2)	$A = 0.08$
Moment arm (m)	$R = 0.1$
Actuation pressure (kPa)	$P_m = 200$–400; $P_p = 0$–P_m
Phase lag (radian)	$\psi = 0, \pi/2, \pi$

As reported previously [29], a_1 is determined by $(T_m - T_{sm})/I_1$. When it is greater than zero, the motion across the frictional interface will be pure slip type although no steady-state responses can be defined since the relative velocity keeps on increasing. However, when $a_1 = 0$ ($T_m = T_{sm}$), steady-state pure slip motions could also take place and the resulting response can be analytically obtained by eliminating the exponentially decaying term in Eq. (14):

$$\dot{\delta}_{1ss}(t) = a_0 + a_{21}\,\sin(\omega t + \varphi_{21}) + a_{22}\,\sin(\omega_f t + \varphi_{22}). \tag{15}$$

Nonetheless, the above-mentioned condition alone cannot warrant pure slip motions. Assuming pure positive slip motions, another condition has to be added to avoid a crossing of zero velocity:

$$|a_0| > |a_{21}| + |a_{22}|. \tag{16}$$

Although a detailed description of the a_0, a_{21} and a_{22} expressions would be lengthy for the time-varying dry friction case, analytical results for the time-invariant dry friction are discussed below for the sake of illustration. When $T_{sp} = 0$ and $T_m = T_{sm}$, Eq. (15) will assume the following expression:

$$\dot{\delta}_1(t) = V_m - \frac{T_p}{I_1\omega}\cos(\omega t) + \frac{T_{sm}}{K_{23}}\frac{2\varsigma}{\omega_n}e^{-\varsigma\omega_n t}\cos(\omega_d t) + \frac{T_{sm}}{K_{23}}\frac{2\varsigma^2 - 1}{\omega_d}e^{-\varsigma\omega_n t}\sin(\omega_d t), \tag{17a}$$

$$\omega_n = \sqrt{K_{23}/I_2}, \quad \varsigma = C_{23}/(2\sqrt{K_{23}I_2}), \quad \omega_d = \omega_n\sqrt{1-\varsigma^2}. \tag{17c–e}$$

Substitute the initial condition $\dot{\delta}_1(0) = \Omega_e$ to obtain V_m, the steady-state response of $\dot{\delta}_{1ss}(t)$ is found as

$$\dot{\delta}_1(t) = (\Omega_e - \frac{T_{sm}}{K_{23}}\frac{2\varsigma}{\omega_n}) + \frac{T_p}{I_1\omega}(1 - \cos(\omega t)). \tag{18}$$

Typical parameters of Table 1 suggest that the term $(T_{sm}2\varsigma)/(K_{23}\omega_n)$ is negligible compared to the engine speed Ω_e, and thus $\dot{\delta}_1(t) = \Omega_e + (T_p/I_1\omega)(1 - \cos(\omega t))$. Thus, the positive definite condition of $\dot{\delta}_1(t)$ ($\dot{\delta}_1(t) > 0 \quad \forall t \in [0, \infty)$) is also satisfied and correspondingly pure positive slip motions are guaranteed. Finally, note that the dynamic amplitude will be dictated by T_p, I_1 and ω.

5. Effect of negative slope friction characteristics with a time-invariant normal load

Duan and Singh had earlier studied the dry friction path problem [22] by assuming $\mu_k = \mu_s$. In this section, we focus more on the steady-state response when $\mu_k \leqslant \mu_s$. Two spectral maps are constructed for examining the effect of μ_k in the frequency domain. The first one is the maximum response vs. frequency ratio map by picking the maximum (max) response amplitude of $\dot{\delta}_1$ at each excitation frequency ω. Further, to illustrate the nonlinear frequency maps, ω is normalized with respect to the linear sub-system natural frequency $\omega_n = \sqrt{K_{23}/I_2}$. The second one is the bifurcation diagram (with ω/ω_n or μ_k/μ_s as a parameter) by picking the values of δ_2 corresponding to starting time of each excitation cycle (i.e. $t = 2\pi n/\omega, n = \text{integer}$). The reason to use δ_2 in constructing the bifurcation diagram is that the variation in δ_2 is relatively smaller than $\dot{\delta}_1$ at the fixed

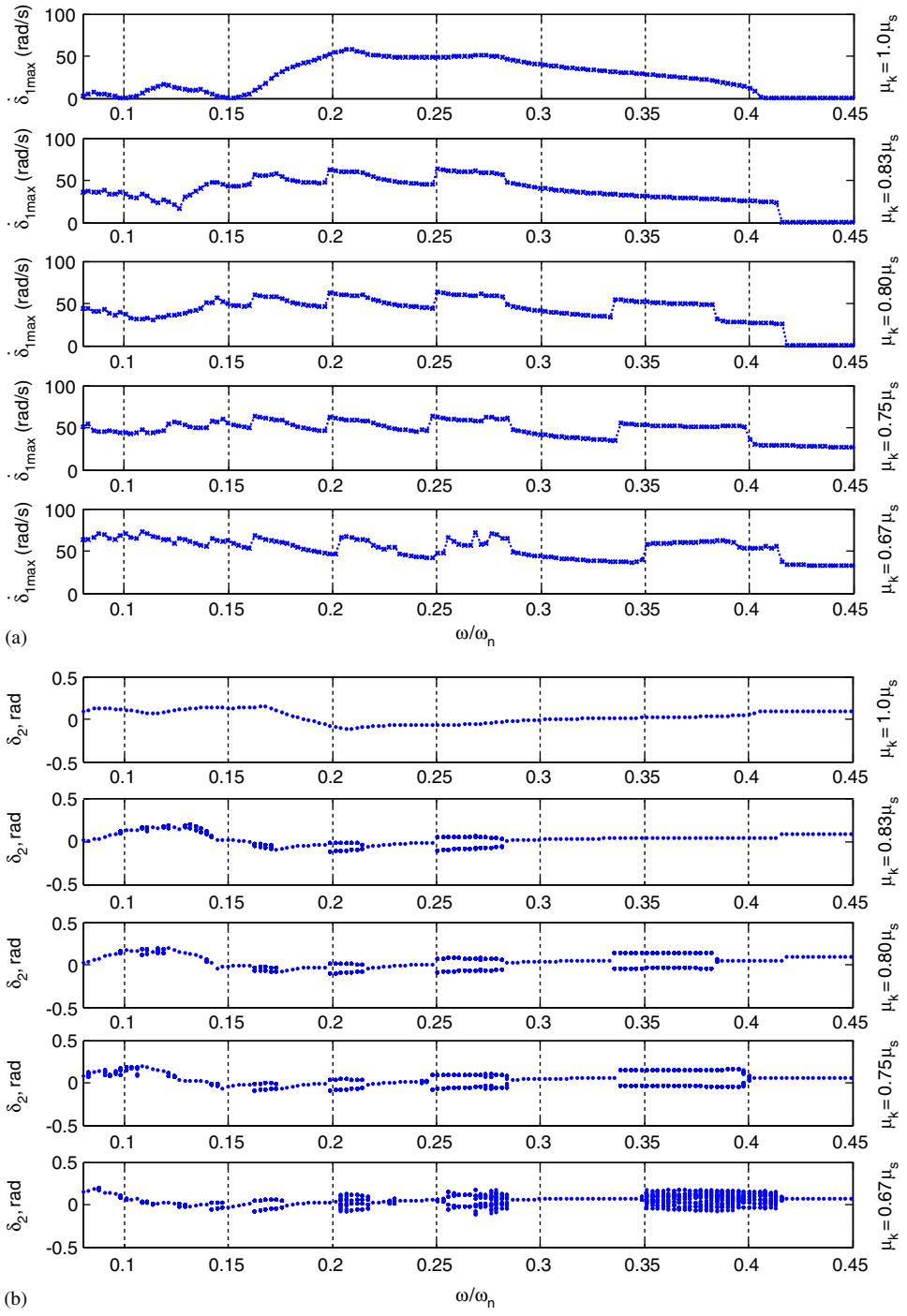

Fig. 4. Effect of μ_k given a time-invariant friction torque: (a) $\delta_{1\max}$ maps; (b) bifurcation diagrams with ω/ω_n as a bifurcation parameter.

phase point. Since a deterministic relationship between δ_2 and $\dot{\delta}_1$ exists, a bifurcation in δ_2 should also indicate a similar response for $\dot{\delta}_1$. To ensure that the steady-state response has been obtained, the first 50 transient cycles in the numerical solution are discarded.

Fig. 4(a) shows the effect of μ_k on $\delta_{1\max}$. When $\mu_k = \mu_s$, the map of $\delta_{1\max}$ is a smooth curve and super-harmonic resonant peaks are not very active. As μ_k is decreased, more super-harmonic resonant peaks around

$\omega/\omega_n = 0.167$, 0.20, 0.25 and 0.33 appear along with jumps. An upward shift in peak frequencies with a decrease in μ_k can be attributed to the "negative damping" effect. Further, the "transition" frequency from pure stick to stick–slip regimes (around $\omega/\omega_n = 0.4$) change with respect to the value of μ_k; this is due to the smoothened friction law as discussed in the previous section. As noted in Fig. 4(b), a jump in $\delta_{1\max}$ yields a corresponding bifurcation point. For example, a jump at $\omega/\omega_n = 0.2$ with $\mu_k = 0.83\mu_s$ changes the period-one motions in to a period-two type. As μ_k is decreased further, the period-two type motions become quasi-periodic or even chaotic responses.

The underlying instability mechanism can be theoretically explained by re-considering the nonlinear friction torque given essentially as a nonlinear damping term. Expand the nonlinear friction torque using the Taylor series and neglect the higher order terms to yield the following where $T_f(\dot{\delta}_0)$ is the instantaneous mean torque:

$$T_f(\dot{\delta}_1) = T_f(\dot{\delta}_{1c}) + \left.\frac{\partial T}{\partial \dot{\delta}}\right|_{\dot{\delta}=\dot{\delta}_{1c}} (\dot{\delta} - \dot{\delta}_{1c}), \tag{19}$$

$$\frac{\partial T}{\partial \dot{\delta}_1} = \mu_k NR \frac{\partial \bar{\mu}}{\partial \dot{\delta}_1}, \tag{20a}$$

$$\frac{\partial \bar{\mu}}{\partial \dot{\delta}_1} = \sigma\left[1.0 + \left(\frac{\mu_s}{\mu_k} - 1.0\right)e^{-\alpha|\dot{\delta}_1|}\right][1.0 - \tanh^2(\sigma\dot{\delta}_1)] - \alpha\left(\frac{\mu_s}{\mu_k} - 1.0\right)e^{-\alpha|\dot{\delta}_1|}\mathrm{sgn}(\dot{\delta}_1)\tanh(\sigma\dot{\delta}_1). \tag{20b}$$

The negative values of $\partial T/\partial\dot{\delta}_1$ are shown in Fig. 3(c). The minimum value decreases with a reduction of μ_k/μ_s. This justifies our choice of μ_k/μ_s as the bifurcation parameter. Conventional approaches to address the stability issues have relied on the absolute value of $\partial T/\partial\dot{\delta}_1$ and have assumed small oscillations [32]. However, this approach would not work for our system because the vibrating amplitude is quite large for a system with significant stick–slip motions as shown in Fig. 2. Instead, we define an equivalent viscous damping (C_f) element by equating the cyclic energy dissipation:

$$C_f \int_0^{\Gamma} \dot{\delta}_1^2 \, \mathrm{d}t = \int_0^{\Gamma} \frac{\partial T}{\partial \dot{\delta}_1} \dot{\delta}_1^2 \, \mathrm{d}t. \tag{21}$$

Re-write the governing Eqs. (1a) and (1b) in the following autonomous form, excluding the excitation and the instantaneous mean friction torque:

$$I_1\ddot{\theta}_1 + C_f(\dot{\delta}_1 - \dot{\delta}_{1c}) = 0, \tag{22a}$$

$$I_2\ddot{\theta}_2 + (C_{23} + C_f)\dot{\theta}_2 + K_{23}\theta_2 - C_f\dot{\theta}_1 = 0. \tag{22b}$$

Observe in the second-order Eq. (22b), that unstable solutions of $\theta_2(t)$ (or $\delta_2(t)$) shall take place whenever the following negative damping condition is satisfied. Under such a condition, $\dot{\theta}_1$ and $\dot{\delta}_1$ also lose stability provided a definite torsional system exists:

$$C_f < -C_{23}. \tag{23}$$

Fig. 5 shows the correlation between the calculated C_f and the bifurcation diagram in the frequency range of 0.08–0.30. Since we have essentially employed a straightforward "brute force" linearization method, it is of course true that we can only partially explain the mechanism of the bifurcations. But, as evident from our numerical results, whenever the C_f crosses the threshold value of -0.6, a bifurcation is observed. In other bifurcation regimes where C_f does not cross the threshold, we may need a more sophisticated method. However, this article focuses on the effect of harmonically varying normal loads and therefore a detailed examination of the role of negative damping and associated bifurcations is left for a future study.

On the other hand, a decrease in the value of μ_k/μ_s further reduces the minimum value of $\partial T/\partial\dot{\delta}_1$. Thus, the resulting equivalent damping C_f will decrease. Fig. 6 illustrates the tendency by employing μ_k/μ_s as a

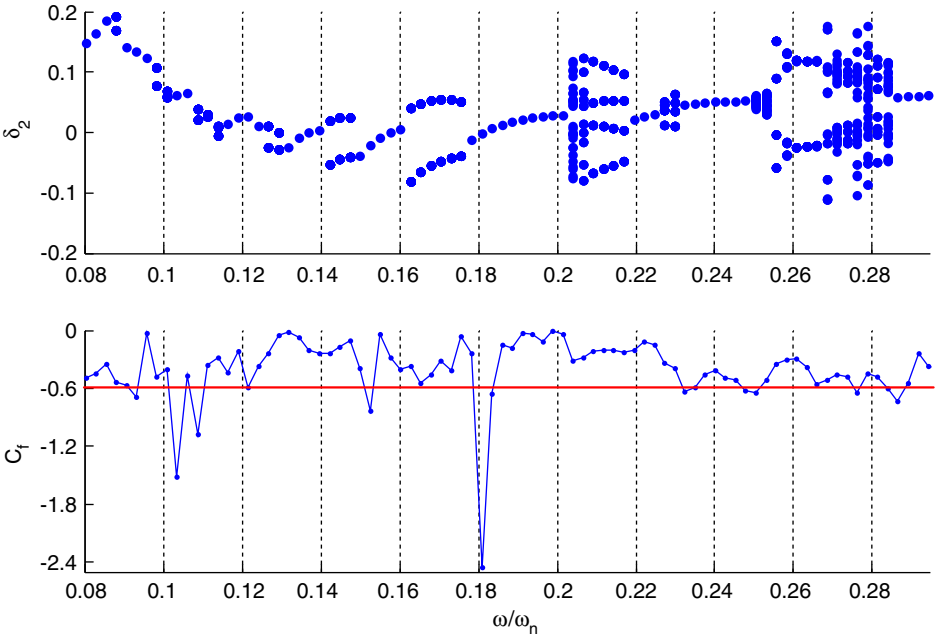

Fig. 5. Correlation between instability regimes and equivalent viscous damping value given $\mu_k = 0.667\mu_s$.

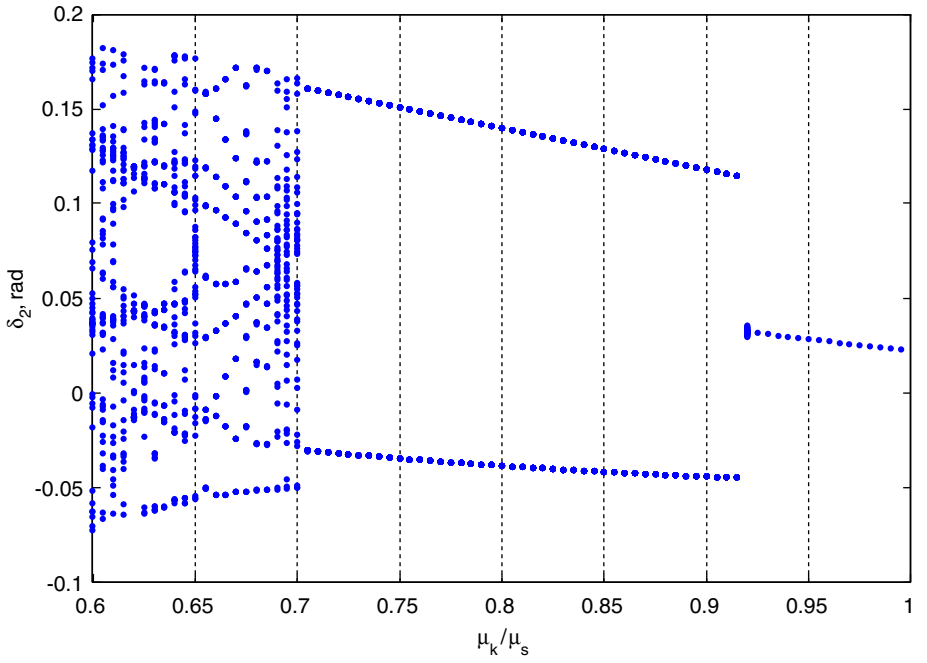

Fig. 6. Bifurcation diagram employing μ_k/μ_s as a bifurcation parameter given $\omega/\omega_n = 0.36$.

bifurcation parameter. As observed, when μ_k/μ_s is closer to unity, only period-one motions are seen. When μ_k/μ_s is decreased to around 0.92, a sudden bifurcation yields period-two type motions. Then as μ_k/μ_s is decreased further down to 0.7, the period-two motions become quasi-periodic or chaotic. Fig. 7 shows the sample time histories of $\dot{\delta}_1$, δ_2 and the Poincare sections corresponding to three values of μ_k/μ_s.

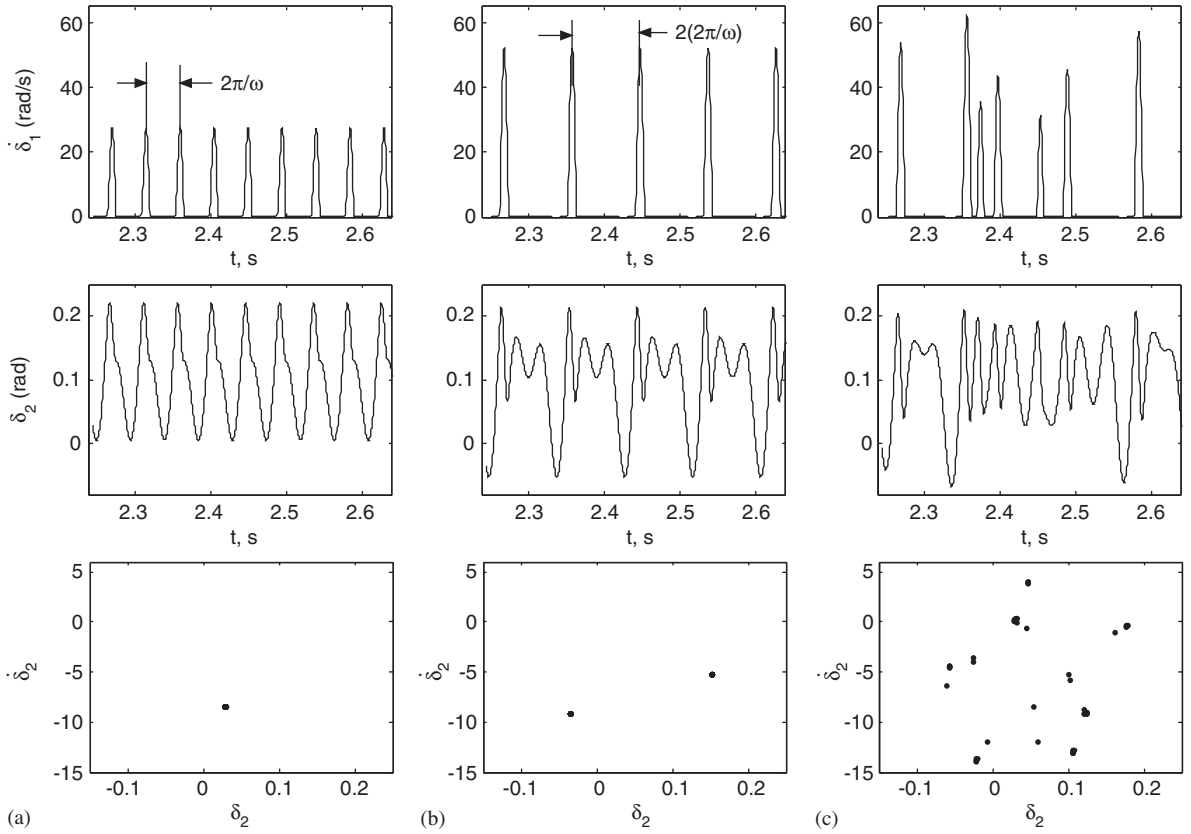

Fig. 7. Sample time histories and Poincare sections given $\omega/\omega_n = 0.36$: (a) $\mu_k/\mu_s = 0.94$, (b) $\mu_k/\mu_s = 0.74$, (c) $\mu_k/\mu_s = 0.64$.

6. Effect of harmonically varying normal load on steady-state behavior

6.1. Effect of actuation parameters ψ, ω_f and T_{sp} with $\mu_k = \mu_s$

Under the condition of $\mu_k = \mu_s$, the effect of phase lag ψ in the actuation pressure is first studied with $\omega_f = \omega$. Fig. 8 shows the max spectral map of $\dot{\delta}_1$ and the corresponding bifurcation diagram with ω/ω_n as a bifurcation parameter. At lower frequencies ($\omega/\omega_n < 0.30$ here) the $\psi = 0$ value yields the best attenuation of stick–slip motions compared with the $\psi = \pi/2$ and π values. This is consistent with our analysis of the transient stick–slip motion as reported in the previous article [29]. But when the frequency is increased, this attenuation effect is reversed since the time-delay in the positive slip response increases. Fig. 9 shows the coupled excitation torque and $\dot{\delta}_1$ response at several frequencies with $T_{sp} = 0$. When the excitation frequency is low ($\omega/\omega_n = 0.15$ and 0.18), the positive slip starts and persists during the first half-cycle of engine torque as shown in Figs. 9(a) and (b). But when the excitation frequency is higher ($\omega/\omega_n = 0.37$ and 0.40), a positive slip is initiated and it continues during the second half of the engine torque cycle as shown in Figs. 9(c) and (d). Differences in the attenuations over different frequency regimes can be analytically explained by assuming semi-positive stick–slip motions. First re-examine Eqs. (8) and (9) of the pure stick case under time-invariant dry friction. Note that the interfacial friction force of Eq. (9) can be also written as follows where $\delta_2(t)$is given by Eq. (8):

$$T_{fi}(t) = I_2\ddot{\delta}_2(t) + C_{23}\dot{\delta}_2(t) + K_{23}\delta_2(t), \tag{24}$$

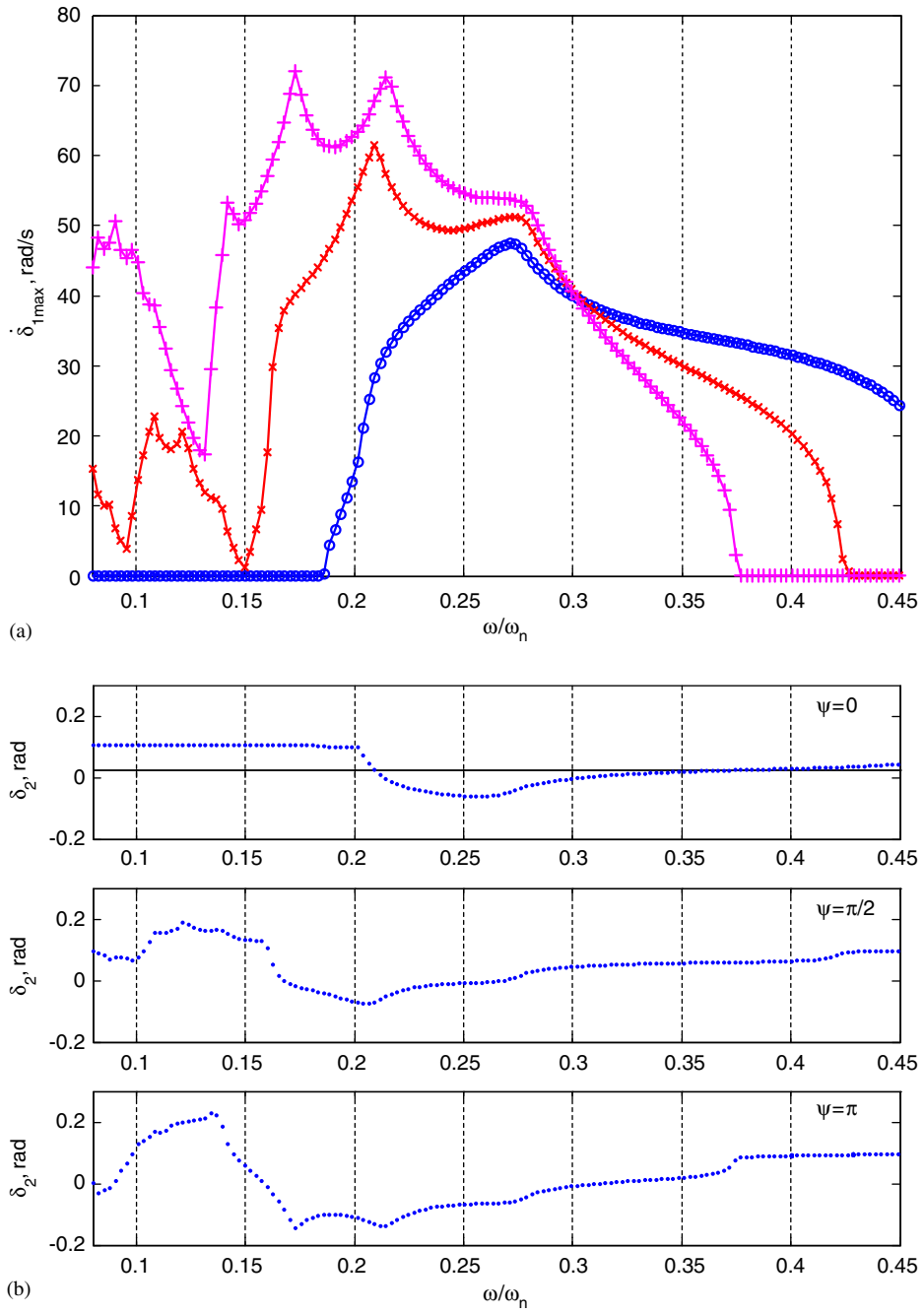

Fig. 8. Effect of phase ψ on the steady-state response given $\omega_f = \omega$ and $T_{sp}/T_{sm} = 0.25$: (a) maximum frequency response map for $\dot{\delta}_1$ with: … ○ … , $\psi = 0$; … × … , $\psi = \pi/2$; … + … , $\psi = \pi$; (b) bifurcation diagram.

$$T_{fi}(t) = T_m + \frac{T_p\sqrt{(K_{23} - I_2\omega^2)^2 + (C_{23}\omega)^2}}{\sqrt{(K_{23} - (I_1 + I_2)\omega^2)^2 + (C_{23}\omega)^2}}\sin(\omega t + \varphi + \vartheta), \tag{25a}$$

$$\vartheta = \tan^{-1}\frac{C_{23}\omega}{K_{23} - I_2\omega^2}. \tag{25b}$$

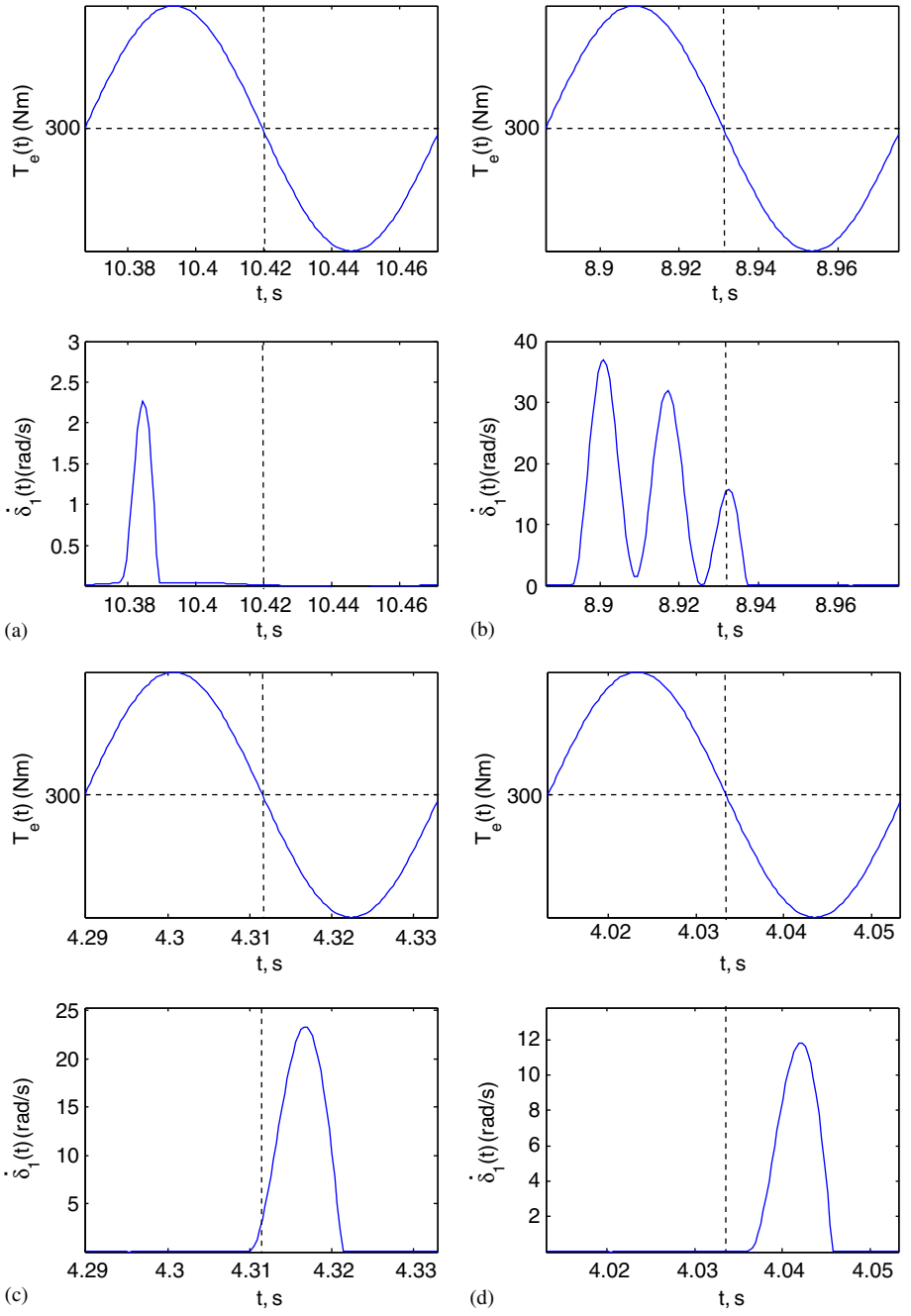

Fig. 9. Time delay in the positive slip motion with respect to the engine torque excitation: (a) $\omega/\omega_n = 0.15$, (b) $\omega/\omega_n = 0.18$, (c) $\omega/\omega_n = 0.37$, (d) $\omega/\omega_n = 0.40$.

Given the system parameters in Table 1, we find that $C_{23}\omega \ll (K_{23} - I_2\omega^2)$ in the frequency range of interest. Thus, $\vartheta \approx 0$ and

$$T_{fi}(t) \approx T_m + \frac{T_p\sqrt{(K_{23} - I_2\omega^2)^2 + (C_{23}\omega)^2}}{\sqrt{(K_{23} - (I_1 + I_2)\omega^2)^2 + (C_{23}\omega)^2}}\sin(\omega t + \varphi). \tag{26}$$

Now the interface friction torque rises with a phase lag φ to the excitation $T_e(t)$. And φ increases from 0° to 180° and crosses the 90° value at the system natural frequency under the pure stick condition

$$\omega_{sn} = K_{23}/\sqrt{I_1 + I_2}. \tag{27}$$

And note the following relationship between ω_{sn} and ω_n given $I_1 = 0.20$ and $I_2 = 0.02$:

$$\frac{\omega_{sn}}{\omega_n} = \frac{\sqrt{I_2}}{\sqrt{I_1 + I_2}} \approx 0.3. \tag{28}$$

This clearly explains the specific boundary dividing the two frequency regimes as illustrated in Fig. 8. As evident from the results, this critical frequency is mainly determined by the system parameters $I_1$and I_2.

On the other hand, under the time-varying condition, the following relationships hold:

$$I_1\ddot{\delta}_1 - \frac{I_1}{I_2}C_{23}\dot{\delta}_2 - \frac{I_1}{I_2}K_{23}\delta_2 = T_{\text{eq}}(t), \tag{29a}$$

$$T_{\text{eq}}(t) = \left[T_m - \left[1.0 + \frac{I_1}{I_2}\right]_{sm}\right] + \left[T_p\,\sin(\omega t) - \left[1.0 + \frac{I_1}{I_2}\right]T_{sp}\,\sin(\omega t + \psi)\right]. \tag{29b}$$

Note a reduction in the equivalent torque excitation leads to a different phase lag ψ. This is similar to the discussion in the previous study on transient responses [29]. As noted, when the positive slip tends to occur during the first-half of the engine torque cycle, $\psi = 0$ provides the maximum decrease in the "effective" excitation T_{eq} and vice versa. Further, all curves in Fig. 8(a) are relatively smooth for the case of $\mu_k = \mu_s$ and no jumps are seen. Accordingly, no bifurcation is observed in Fig. 8(b).

Second, the effect of ω_f is shown in Figs. 10 and 11. As seen in Figs. 10(a) and 11(a), best attenuation of the slip motion occurs at lower frequencies as $\omega_f = \omega$. This effect is however reversed when ω is increased. An explanation can be found in a manner similar to the case discussed above, but with different values of ψ. Also, no bifurcations seem to take place in Figs. 10(b) and 11(b). Let us assume that $\omega_f = M\omega/N$ where both M and N are integers and ω is the engine excitation frequency. It is noted that it does not matter whether M and N are commensurable or not, the resulting motions will possess a period identical to ω/N. For example, when M/N is 1/2, then the motions are of period-two type; when M/N is 2/1, the motions are of period-one type as shown in Fig. 10(b); when $M/N = 2/3$, the motions are of period-three type; and when $M/N = 4/3$, the motions are also of period-three type as shown in Fig. 11(b). Time histories in Fig. 12 confirm such results. This phenomenon can be explained via the harmonic balance analysis. For a period—N ($N \geqslant 1$) time-varying actuation, assume periodic-υ ($\upsilon \geqslant 1$) solution of $\dot{\delta}_1(t)$ as a truncated Fourier series where $\omega_0 = \omega/\upsilon$ is the fundamental frequency component:

$$\dot{\delta}_1(t) = \sum_{n=1}^{N_h} a_n\,\cos(n\omega_0 t) + b_n\,\sin(n\omega_0 t). \tag{30}$$

Thus, the NLTV friction torque can be written in the following form where c_n and d_n expression are Fourier coefficients of $\bar{\mu}(\dot{\delta}_1)$. Further, assume $M = 1$ without a loss of generality:

$$T_f(t) = \left(T_m + T_p\,\sin\left(\frac{1}{N}\omega\right)\right)\left(\sum_{n=1}^{N_h} c_n\,\cos(n\omega_0 t) + d_n\,\sin(n\omega_0 t)\right). \tag{31}$$

Substitute Eqs. (30) and (31) into Eq. (1) to yield the following, where the coefficients f_n, g_n, r_n and s_n are undetermined constants:

$$\sum_{n=1}^{N_h}\left[f_n\,\cos(n\omega_0 t) + g_n\,\sin(n\omega_0 t)\right] + \sin\left(\frac{1}{N}\omega t\right)\sum_{n=1}^{N_h}\left[r_n\,\cos(n\omega_0 t) + s_n\,\sin(n\omega_0 t)\right] = T_m + T_p\,\sin(\omega t). \tag{32}$$

The following trigonometric relationships hold:

$$\sin\left(\frac{1}{N}\omega t\right)\cos(n\omega_0 t) = \frac{1}{2}\left\{\sin\left[\left(\frac{n}{\upsilon} + \frac{1}{N}\right)\omega t\right] - \sin\left[\left(\frac{n}{\upsilon} - \frac{1}{N}\right)\omega t\right]\right\}, \tag{33a}$$

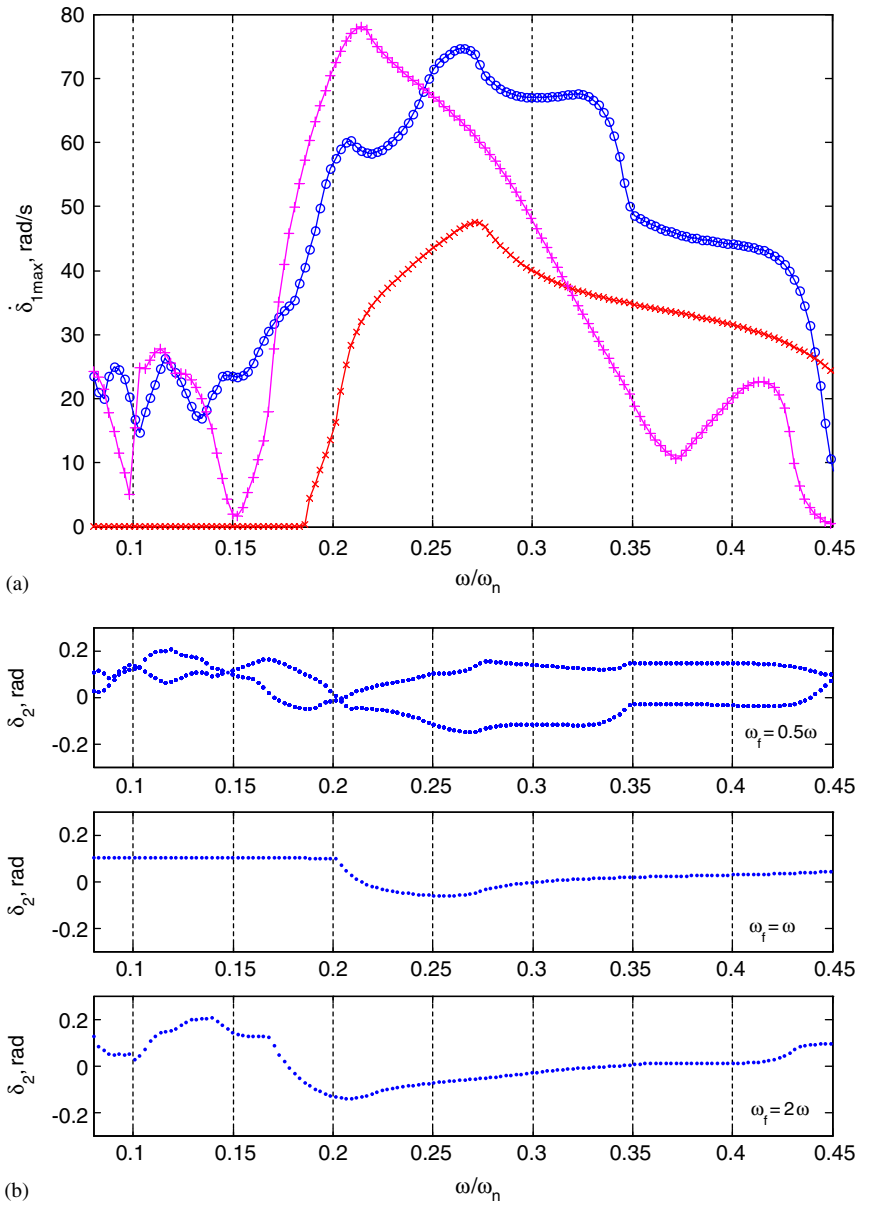

Fig. 10. Effect of ω_f on the steady-state response given $\psi = 0$ and $T_{sp}/T_{sm} = 0.25$: (a) maximum frequency response map for $\dot{\delta}_1$ with: $\ldots\circ\ldots$, $\omega_f = 0.5\omega$; $\ldots\times\ldots$, $\omega_f = \omega$; $\ldots+\ldots$, $\omega_f = 2.0\omega$; (b) bifurcation diagram.

$$\sin\left(\frac{1}{N}\omega t\right)\sin(n\omega_0 t) = \frac{1}{2}\left\{\cos\left[\left(\frac{n}{\upsilon}-\frac{1}{N}\right)\omega t\right] - \cos\left[\left(\frac{n}{\upsilon}+\frac{1}{N}\right)\omega t\right]\right\}. \tag{33b}$$

Eq. (32) can be further simplified as follows where λ_{1n}, λ_{1n} and λ_{3n} are the Fourier coefficients and Θ_n, Ψ_n and Υ_n are corresponding phase angles:

$$\sum_{n=1}^{N_h}\left[\lambda_{1n}\sin\left(\frac{n}{\upsilon}\omega t + \Theta_n\right)\right] + \sum_{n=1}^{N_h}\begin{bmatrix}\lambda_{2n}\sin\left(\left(\frac{n}{\upsilon}-\frac{1}{N}\right)\omega t + \Psi_n\right)\\ +\lambda_{3n}\sin\left(\left(\frac{n}{\upsilon}+\frac{1}{N}\right)\omega t + \Upsilon_n\right)\end{bmatrix} = T_m + T_p\sin(\omega t). \tag{34}$$

On the left-hand side (LHS) of Eq. (34), the first term is contributed by the mean term of friction torque and the second term by the alternating $T_{sp}(t)$. The right-hand side (RHS) is the periodic excitation. According to

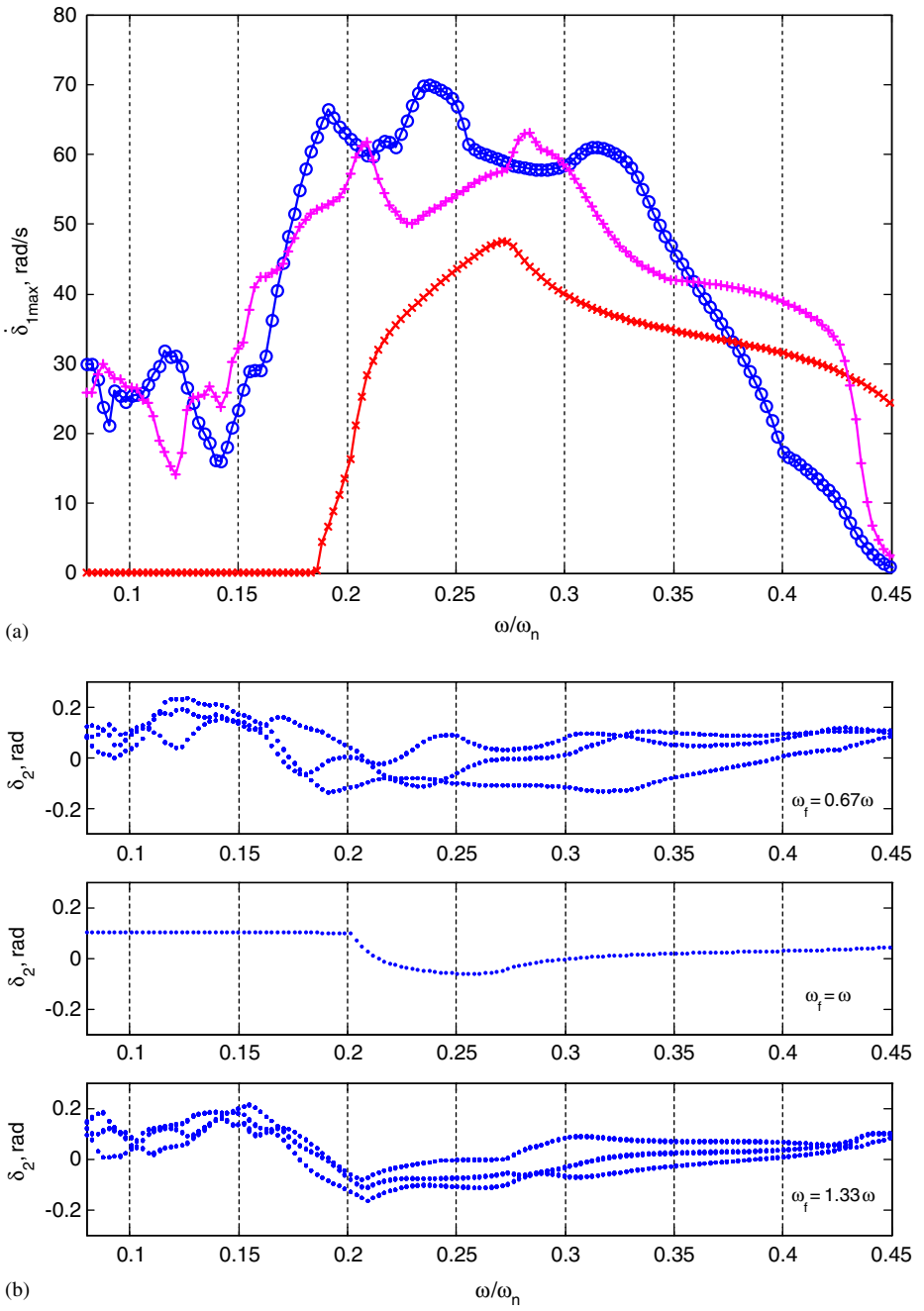

Fig. 11. Effect of ω_f on the steady-state response given $\psi = 0$ and $T_{sp}/T_{sm} = 0.25$: (a) maximum frequency response map for $\dot{\delta}_1$ with: $\ldots\circ\ldots$, $\omega_f = 0.667\omega$; $\ldots\times\ldots$, $\omega_f = \omega$; $\ldots+\ldots$, $\omega_f = 1.33\omega$; (b) bifurcation diagram.

Eq. (34), given an arbitrary choice of integer N, the following relationship must hold:

$$\upsilon = N. \tag{35}$$

To prove the above conclusion, first assume υ and N are incommensurable, to satisfy the periodicity and like harmonic terms on the LHS and RHS of Eq. (34). The second term on the LHS needs to be self-balanced to zero. However, that would indicate that the alternating $T_{sp}(t)$ has no effect on the overall system response but

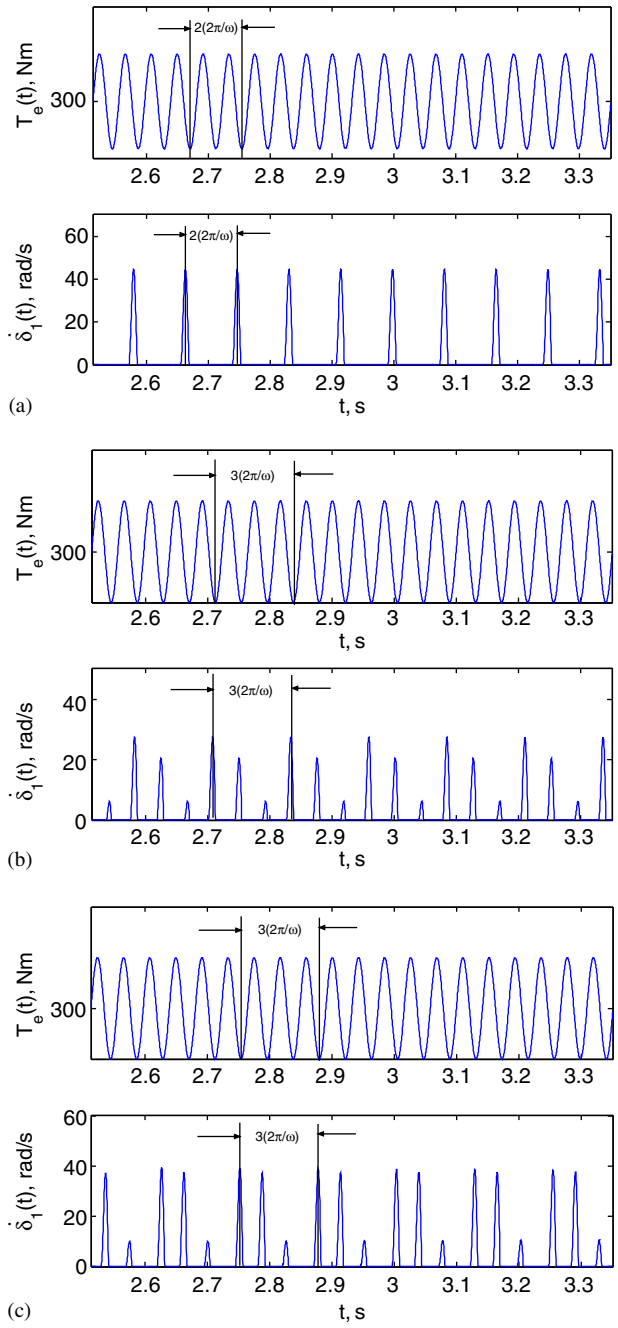

Fig. 12. Sample time histories for different ω_f given $\omega = 150$, $T_{sp}/T_{sm} = 1/4$: (a) $\omega_f = 0.5\omega$, (b) $\omega_f = 0.67\omega$, (c) $\omega_f = 1.33\omega$.

this is not true from the physical perspective. Second, assume υ and N are commensurable (but not identical, i.e. $N = K\upsilon$ where K is an integer), the same requirement as for the incommensurable case is applied to the second term on the LHS of Eq. (34). The other situation corresponding to $\upsilon = KN$ is disregarded here since only the minimum period defines the periodicity. This reveals an interesting phenomenon: under a time-varying actuation pressure with period—N, the resulting nonlinear response exhibits the same frequency as the system would under a dual frequency (1 and M/N) excitation.

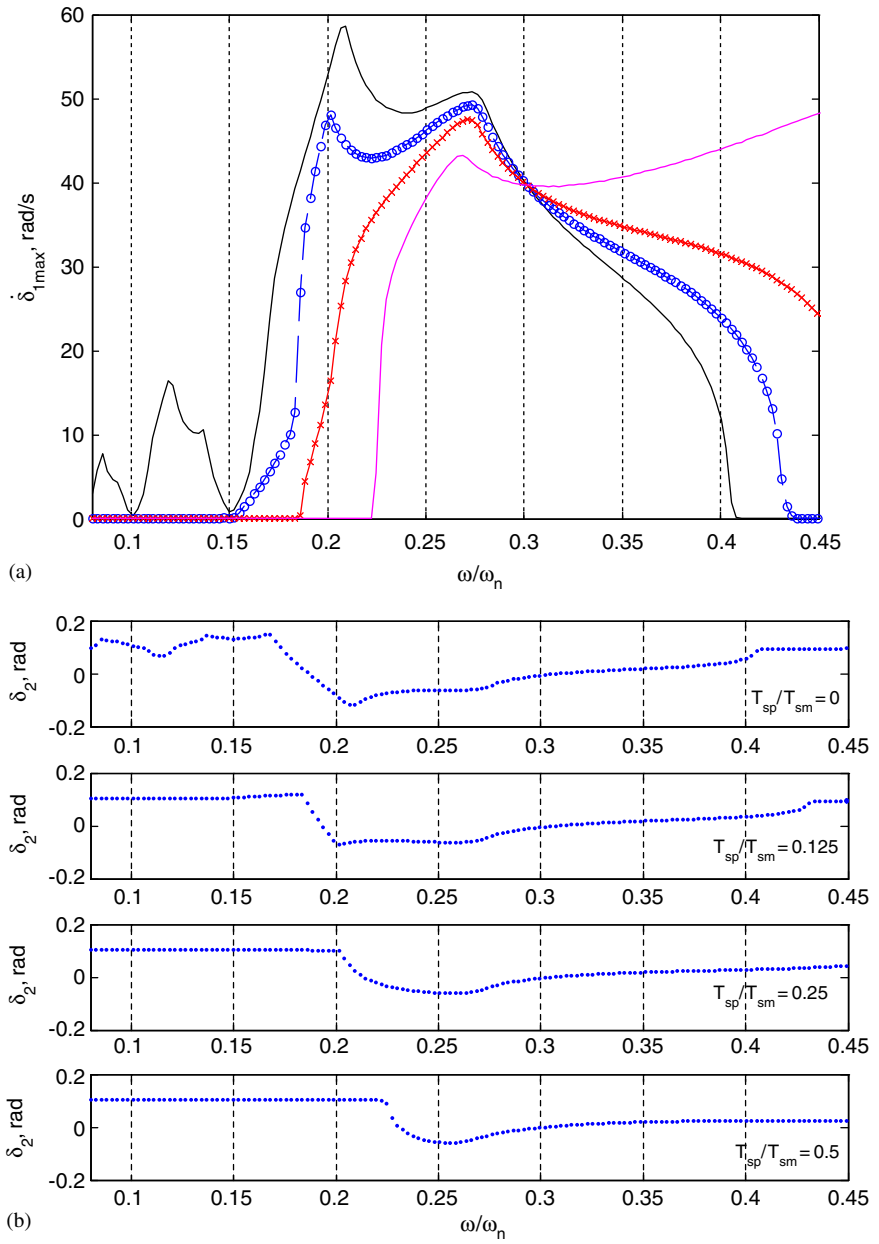

Fig. 13. Effect of ω_f on the steady-state response given $\psi = 0$ and $\omega_f = \omega$: (a) maximum frequency response map for $\dot{\delta}_1$ with: ___ , $T_{sp}/T_{sm} = 0$; … ○ …, $T_{sp}/T_{sm} = 0.125$; … × … , $T_{sp}/T_{sm} = 0.25$; _.._, $T_{sp}/T_{sm} = 0.50$; (b) bifurcation diagram.

Last, the effect of T_{sp} is studied given $\omega_f = \omega$ and $\psi = 0$. Fig. 13 shows the corresponding max spectral maps and bifurcation diagram. Consistent with the above-mentioned analyses, a higher value of T_{sp} provides the best attenuation of the slip motions at lower frequencies, but this effect is reversed at higher frequencies. Again, no bifurcation and quasi-periodic or chaotic motions are generated.

6.2. *Interaction between negative slope $\mu(\dot{\delta}_1)$ and harmonically varying $N(t)$*

First, the interaction between $\mu(\dot{\delta}_1)$ and ψ is investigated under the condition $\omega_f = \omega$ and $T_{sp}/T_{sm} = 0.25$. Fig. 14 shows the resulting max spectral maps and bifurcation diagram with $\psi = 0$, $\pi/2$ and π, given

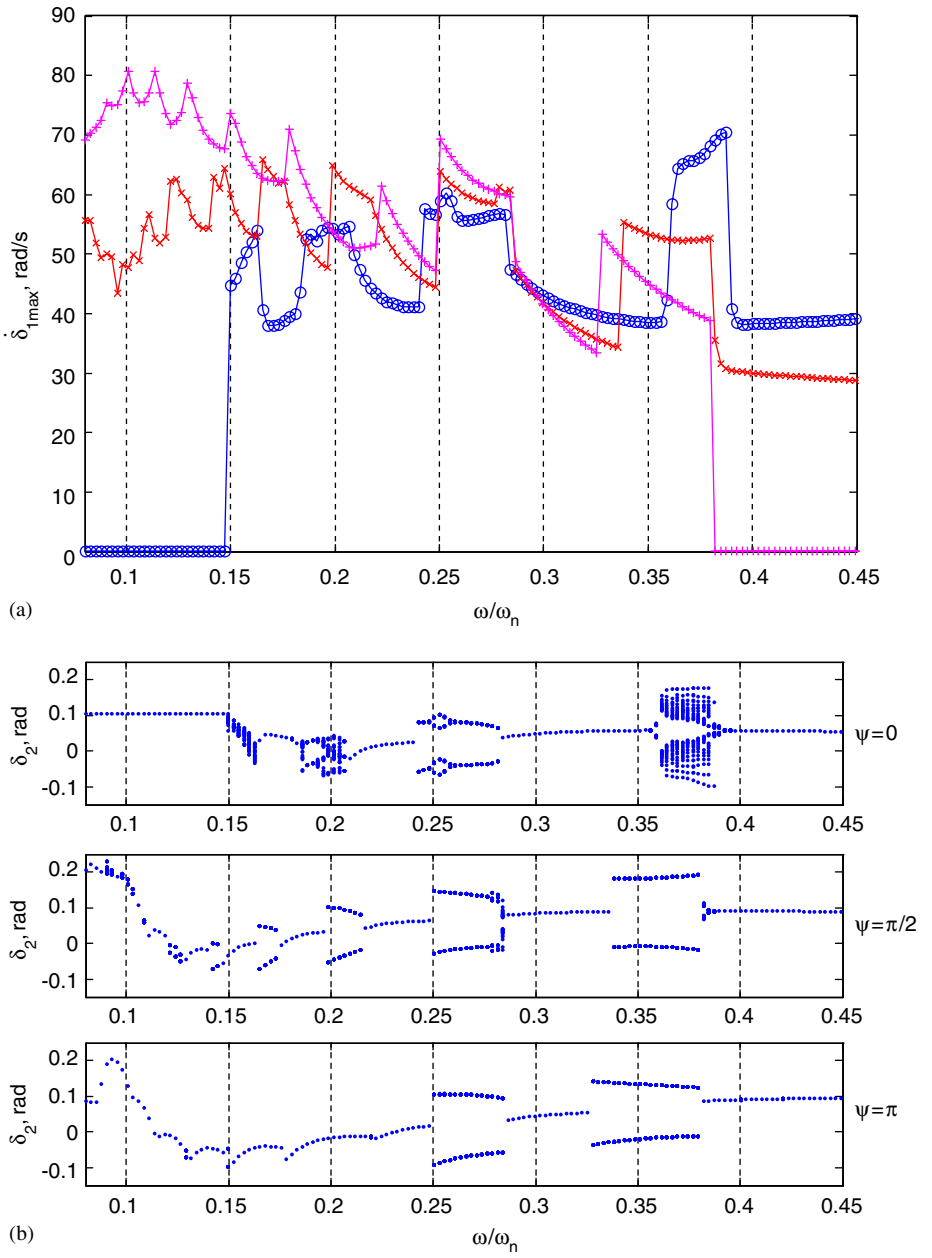

Fig. 14. Interaction between $\mu_k(\dot{\delta}_1)$ and ψ given $T_{sp}/T_{sm} = 0.25$, $\omega_f = \omega$ and $\mu_k = 0.75\mu_s$: (a) maximum frequency response maps of $\dot{\delta}_{1\,\max}$ with: … ○ … , $\psi = 0$; … × … , $\psi = \pi/2$; … + … , $\psi = \pi$; (b) bifurcation diagram.

$\mu_k = 0.75\mu_s$. The combined effects of the negative damping phenomenon and varying phases (or time delays) are clearly observed in Fig. 14(a). The negative damping introduces active super-harmonic peaks, similar to Fig. 4(a). Further, three values of ψ seem to produce the same attenuation effect in the slip motion as the case $\mu_k = \mu_s$ yielded in Fig. 8(a). The $\psi = 0$ phase lag has the best attenuation at lower ω but it acts in an opposite way at higher ω. When $\psi = 0$, only the pure stick motions exist when $\omega/\omega_n < 0.15$. Consequently, only the period-one type motions occur in this regime. Note that the transition occurs at a lower value of ω/ω_n than that observed (around 0.18) in Fig. 8(a). This could be attributed to an amplification that is induced by the negative damping. As ω is increased further, super-harmonic peaks appear with jumps. Such jumps would

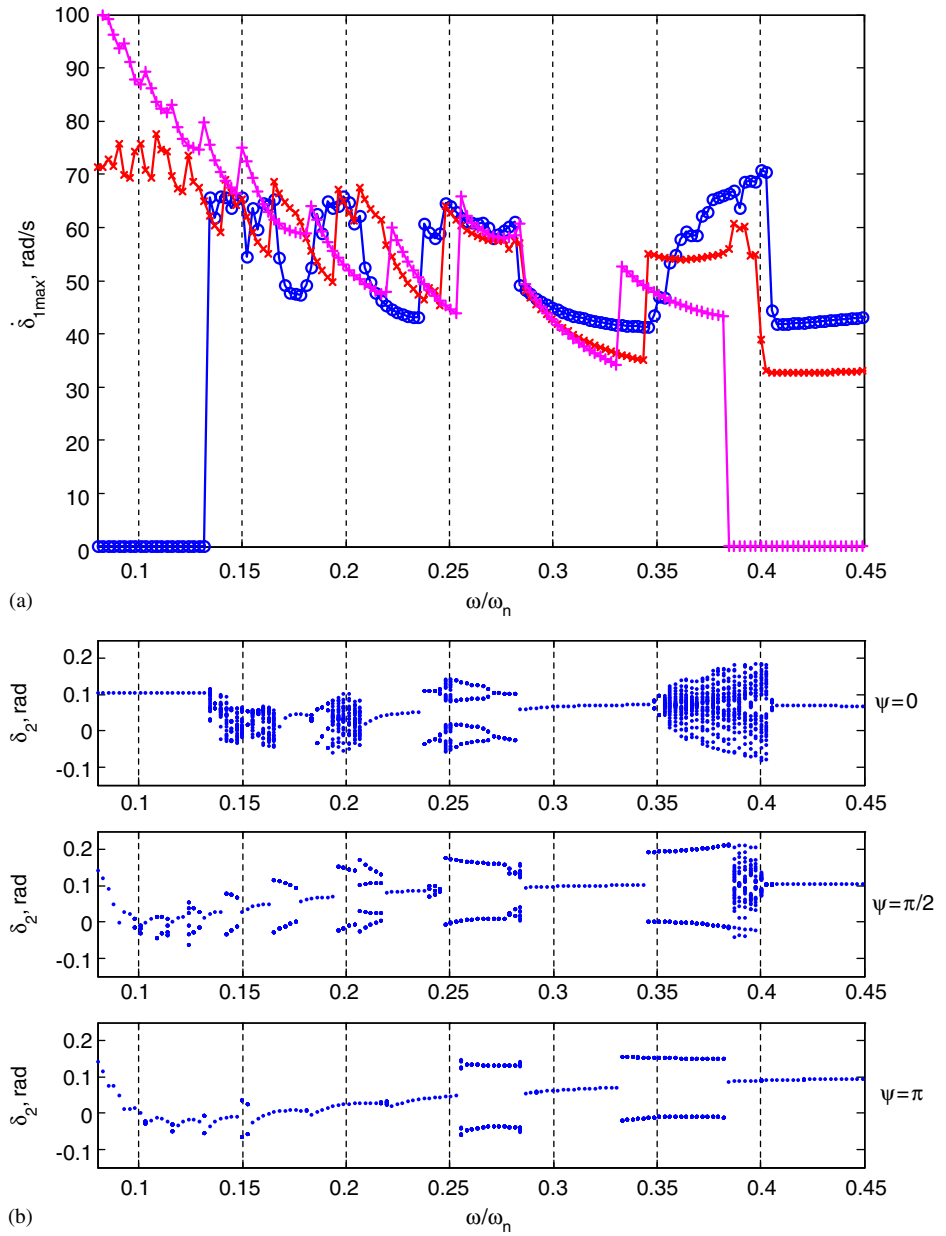

Fig. 15. Interaction between $\mu_k(\dot{\delta}_1)$ and ψ given $T_{sp}/T_{sm} = 0.25$, $\omega_f = \omega$ and $\mu_k = 0.67\mu_s$: (a) maximum frequency response maps of $\dot{\delta}_{1\,max}$: … ○ … , $\psi = 0$; … × … , $\psi = \pi/2$; … + … , $\psi = \pi$; (b) bifurcation diagram.

certainly indicate a loss in the stability and thus bifurcations are found in Fig. 14b. The severity of bifurcations seems to be more dependent on the abruptness of jumps than the amplitudes of slip motions. As noted in Fig. 14(a), a significant jump occurs around $\omega/\omega_n = 0.35$ given $\psi = 0$; consequently the periodic motions become chaotic. In contrast, the slip motions for $\psi = \pi$ are higher at lower ω, but the peaks now occur in relatively smooth manner and accordingly no bifurcations are seen. Similar phenomena are observed in Fig. 15 except that more bifurcations and quasi-periodic or chaotic motions occur as a result of a further decrease in the value of μ_k.

Second, the effect of μ_k with several ω_f values is studied given $\psi = 0$ and $T_{sp}/T_{sm} = 0.25$. Resulting max spectral maps and bifurcation diagrams are shown in Figs. 16 and 17. Again, the combined effects of negative

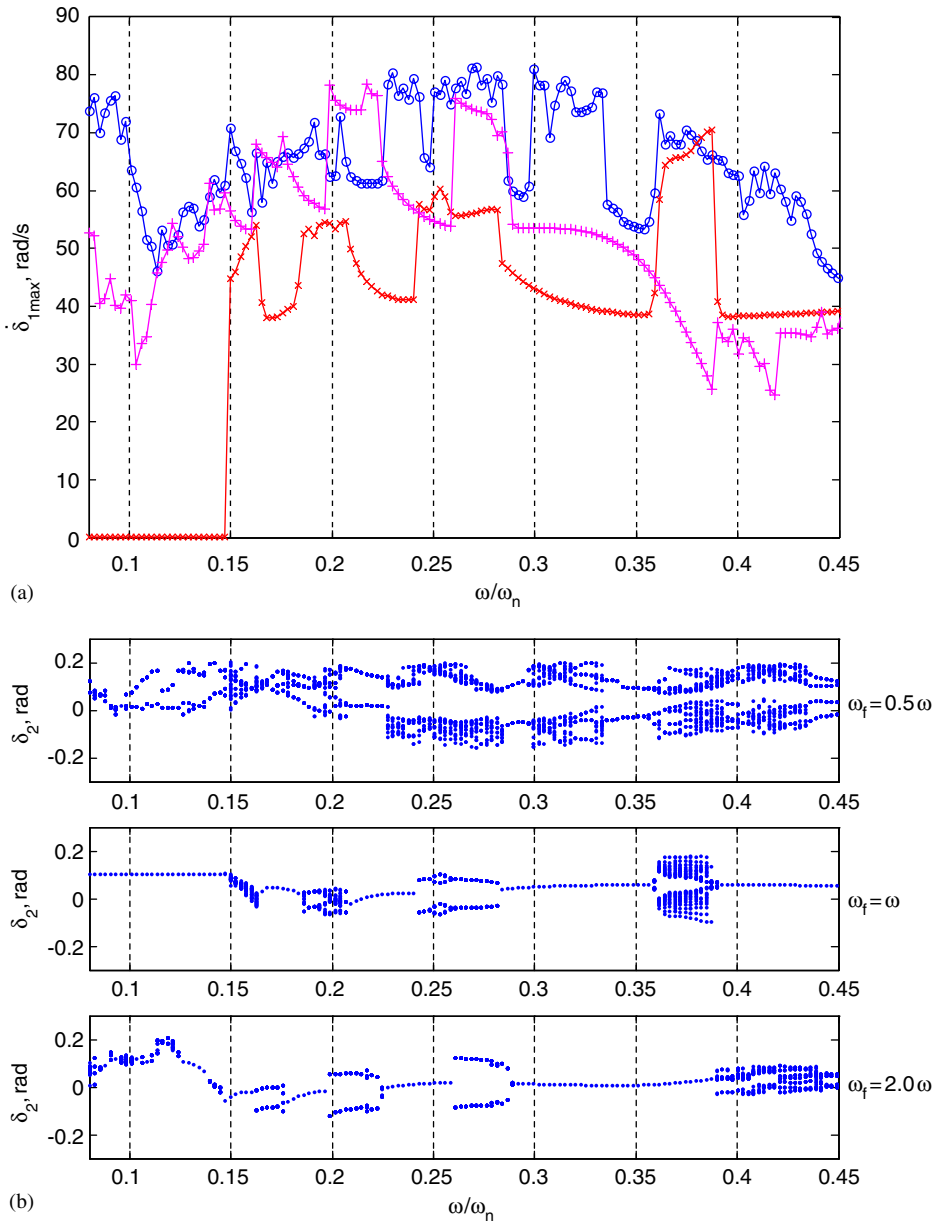

Fig. 16. Interaction between $\mu_k(\dot{\delta}_1)$ and ω_f given $T_{sp}/T_{sm} = 0.25$, $\psi = 0$ and $\mu_k = 0.75\mu_s$: (a) maximum frequency response maps of $\dot{\delta}_{1\,\max}$ with: … ○ … , $\omega_f = 0.5\omega$; … × … , $\omega_f = \omega$; … + … , $\omega_f = 2\omega$; (b) bifurcation diagram.

damping and mismatched frequencies ω_f are clearly evident. At lower ω, the friction torque with $\omega_f = \omega$ suppresses the slip motions better than the $\omega_f = 2\omega$ case does. Numerous jumps take place in the particular case of $\omega_f = 0.5\omega$ in Fig. 16, and quasi-periodic or chaotic motions seem to prevail over the entire frequency range of interest. Similarly, Fig. 18 presents results with several values of T_{sp} under the $\omega_f = \omega$ and $\psi = 0$ condition. As a result of increased attenuation with T_{sp} in Fig. 18(a), initial quasi-periodic or chaotic motions at lower ω become period-one type at the transition from stick–slip to pure stick motions as shown in Fig. 18(b). However, enhanced slip motions and enlarged jumps convert the periodic motions back into quasi-periodic or chaotic ones at higher ω, say around 0.25 and 0.35.

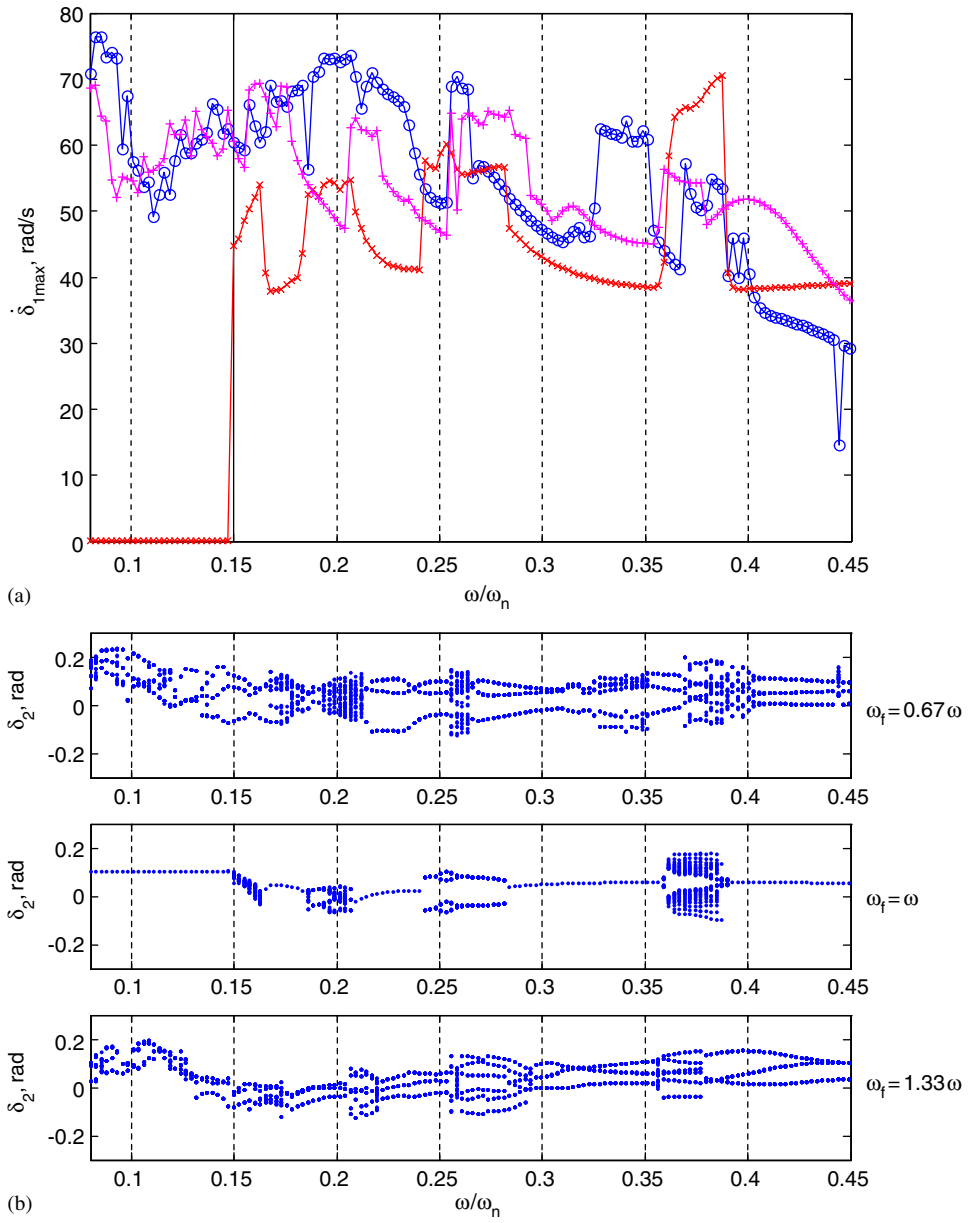

Fig. 17. Interaction between $\mu_k(\dot{\delta}_1)$ and ω_f given $T_{sp}/T_{sm} = 0.25$, $\psi = 0$ and $\mu_k = 0.75\mu_s$: (a) maximum frequency response maps of $\dot{\delta}_{1\,max}$ with: … ○ … , $\omega_f = 0.67\omega$; … × … , $\omega_f = \omega$; … + … , $\omega_f = 1.33\omega$; (b) bifurcation diagram.

7. Conclusion

Effects of harmonically varying normal load on the steady-state responses of a torsional system with dry friction path have been studied. To the best of our knowledge, no prior researcher has addressed such an NLTV friction force or torque issue, with the exception of sliding friction issues in gears in which the periodically varying friction acts in the off-line-of-action while the mesh force excitation is along the line-of-action [11,12]. Two further contributions of our article emerge. The nature of steady-state response, for example, pure stick, pure slip and stick–slip motions, has been analytically defined and determined. Second, the effects of time-varying friction on steady-state responses have been analytically and numerically studied.

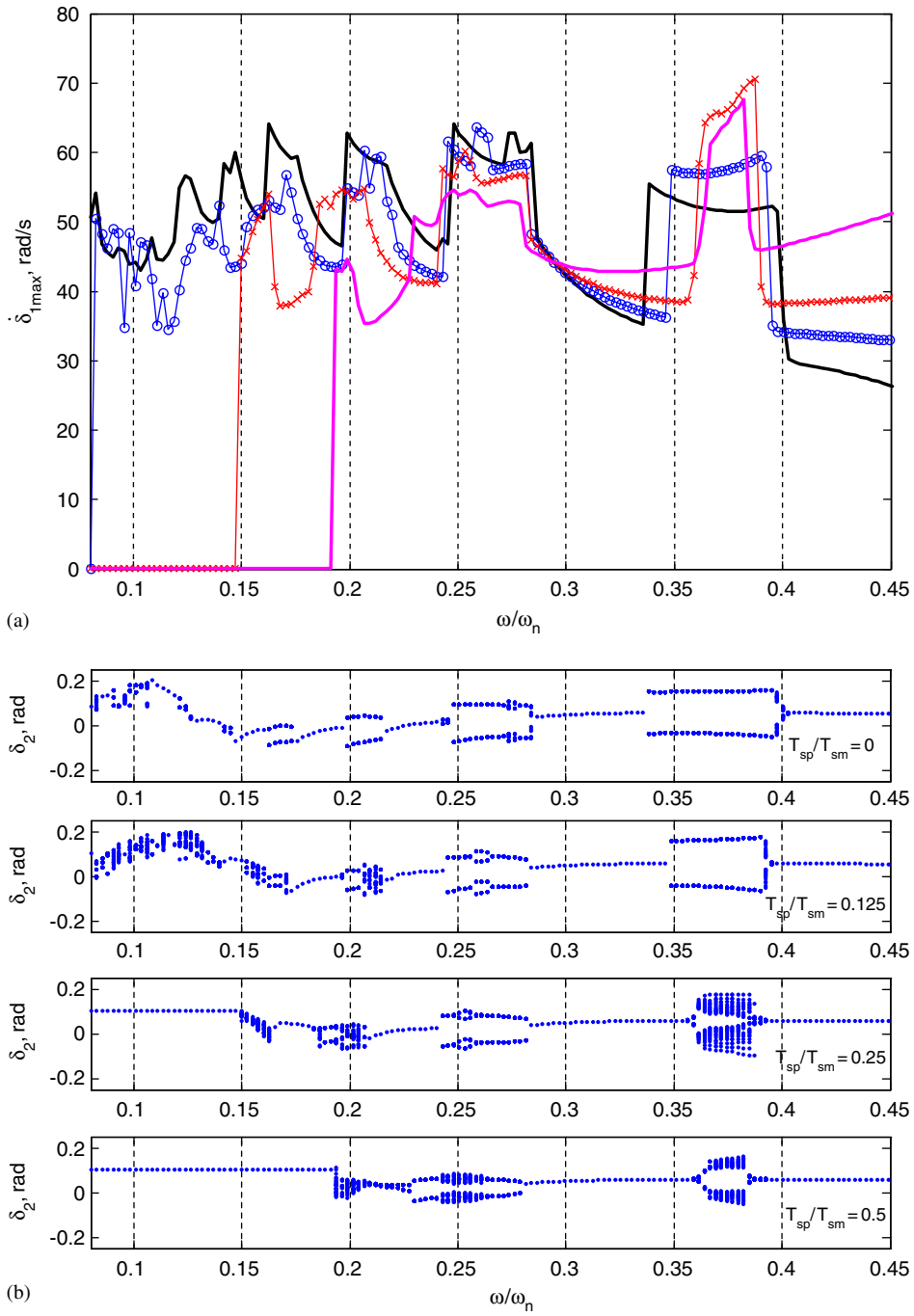

Fig. 18. Interaction between $\mu_k(\dot{\delta}_1)$ and T_{sp} given $\omega_f = \omega$, $\psi = 0$ and $\mu_k = 0.75\mu_s$: (a) maximum frequency response maps of $\dot{\delta}_{1\max}$ with: ___, $T_{sp}/T_{sm} = 0$; … ○ … , $T_{sp}/T_{sm} = 0.125$; … × … , $T_{sp}/T_{sm} = 0.25$; _.._, $T_{sp}/T_{sm} = 0.5$; (b) bifurcation diagram.

Results show that the actuation system parameters ψ, ω and T_{sp} can possibly attenuate the system response. Analytical study has clearly shown the different attenuations seen at lower and higher frequency regime and these have been confirmed by the numerical results. Bifurcation diagram are constructed to detect qualitative changes in the dynamic behavior. The negative slope in μ is the major cause of bifurcations and quasi-periodic or chaotic responses. Around the super-harmonic peak frequencies, the nonlinear system tends to lose stability

in the form of an abrupt jump in the max spectral maps of $\dot{\delta}_1$ and consequently bifurcations take place. An equivalent viscous damping term is considered to analytically investigate the instability issues. Further, the periodicity of the system response under harmonically varying actuation is examined by employing the harmonic balance method. Finally, some suggestions for future work are outlined. A more efficient computational solution method for the NLTV problem must be developed since numerical stiffness issues are encountered. A path following or parametric continuation study should assist in systematically identifying the nature of the bifurcations.

Acknowledgment

Financial support through the DaimlerChrysler Challenge Fund is gratefully acknowledged.

References

[1] J.P. Den Hartog, Forced vibrations with combined Coulomb and viscous friction, *Transaction of the ASME*, APM-53-9, 1931, pp. 107–115.
[2] T.K. Pratt, R. Williams, Nonlinear analysis of stick/slip motion, *Journal of Sound and Vibration* 74 (4) (1981) 531–542.
[3] S.W. Shaw, On the dynamic response of a system with dry friction, *Journal of Sound and Vibration* 108 (2) (1986) 305–325.
[4] A.A. Ferri, Friction damping and isolation systems, *Transaction of the ASME*, *Special 50th Anniversary Design Issue*, Vol. 117, June 1995, pp. 196–206.
[5] B.L. Van De Vrande, D.H. Van Campen, A. De Kraker, An approximate analysis of dry-friction-induced stick–slip vibration by a smoothing procedure, *Nonlinear Dynamics* 19 (1999) 157–169.
[6] R.L. Leine, D.H. Van Campen, A. De Kraker, Stick–slip vibrations by alternate friction models, *Nonlinear Dynamics* 16 (1) (1998) 41–54.
[7] A. Hartung, H. Schmieg, P. Vielsack, Passive vibration absorber with dry friction, *Archive of Applied Mechanics* 71 (2001) 463–472.
[8] D. Karnopp, Computer simulation of stick–slip friction in mechanical dynamic systems, *Transaction of the ASME, Journal of Dynamic Systems, Measurement, and Control* 107 (1985) 100–103.
[9] E.J. Berger, Friction modeling for dynamic system simulation, *Applied Mechanics Reviews* 55 (6) (2002) 535–577.
[10] B. Feeny, F.C. Moon, Chaos in a forced dry-friction oscillator: experiments and numerical modeling, *Journal of Sound and Vibration* 170 (3) (1994) 303–323.
[11] M. Vaishya, R. Singh, Sliding friction induced non-linearity and parametric effects in gear dynamics, *Journal of Sound and Vibration* 248 (4) (2001) 671–694.
[12] M. Vaishya, R. Singh, Analysis of periodically varying gear mesh systems with coulomb friction using floquet theory, *Journal of Sound and Vibration* 243 (3) (2001) 525–545.
[13] A. Albers, Torque control isolation (TCI) the smart clutch, *Fourth International Luk Symposium*, Baden-Baden (Germany), April 20, 1990, pp. 81–107.
[14] R. Berger, R. Meinhard, B. Carsten, The parallel shift gearbox PSG, twin clutch gearbox with dry clutches, *Luk Symposium*, 2002, pp. 197–210.
[15] M. Goetz, M.C. Levesley, D.A. Crolla, Dynamic modeling of a twin clutch transmission for controller design, *Proceedings of the Fifth International Conference on Modern Practice in Stress and Vibration Analysis*, *Material Science Forum*, Vol. 440–441, 2003, pp. 253–260.
[16] R. Fischer, D. Otto, Torque converter clutch systems, *The Fifth Luk Symposium*, May 1994, pp. 107–138.
[17] Personal discussions with automotive powertrain engineers, 2002.
[18] K. Kono, H. Itoh, S. Nakamura, K. Yoshizawa, Torque converter clutch slip control system, *SAE Paper* 950672, 1995.
[19] T. Hiramatsu, T. Akagi, H. Yoneda, Control technology of minimal slip-type torque converter clutch, *SAE* 850460, 1986.
[20] J. Hahn, K. Lee, Nonlinear robust control of torque converter clutch slip system for passenger vehicles using advanced torque estimation algorithms, *Vehicle System Dynamics* 37 (3) (2002) 175–192.
[21] C. Duan, R. Singh, Stick–slip behavior in torque converter clutch, *SAE Noise and Vibration Conference*, 2005-01-2456, 2005.
[22] C. Duan, R. Singh, Super-harmonics in a torsional system with dry friction path subject to harmonic excitation under a mean torque, *Journal of Sound and Vibration* 285 (4–5) (2005) 803–834.
[23] R. Singh, H. Xie, R.J. Comparin, Analysis of automotive neutral gear rattle, *Journal of Sound and Vibration* 131 (2) (1989) 177–196.
[24] B. Ermentrout, *Simulating, Analyzing, and Animating Dynamical Systems: a Guide to XPPAUT for Researchers and Students*, SIAM, Philadelphia, PA, 2002.
[25] T.C. Kim, T.E. Rook, R. Singh, Effect of smoothening functions on the frequency response of an oscillator with clearance non-linearity, *Journal of Sound and Vibration* 263 (2003) 665–678.
[26] G.W. Blankenship, A. Kahraman, Steady-state forced response of a mechanical oscillator with combined parametric excitation and clearance type non-linearity, *Journal of Sound and Vibration* 185 (5) (1995) 743–765.
[27] T.C. Kim, T.E. Rook, R. Singh, Super- and sub-harmonic response calculations for a torsional system with clearance non-linearity using the harmonic balance method, *Journal of Sound and Vibration* 281 (3–5) (2005) 965–993.

[28] J.R. Dormand, P.J. Prince, A family of embedded Runge–Kutta formulae, *Journal of Computational and Applied Mathematics* 6 (1) (1980) 19–26.
[29] C. Duan, R. Singh, Transient responses of a 2DOF torsional system with non-linear dry friction under a time-varying normal load, *Journal of Sound and Vibration* 285 (4–5) (2005) 1223–1234.
[30] www.math.pitt.edu/∼bard/xpp/help/xppauto.html.
[31] C. Duan, R. Singh, Dynamics of a 3DOF torsional system with a dry friction controlled path, *Journal of Sound and Vibration* 289 (4–5) (2006) 657–688.
[32] N. Yamada, K. Ando, An analysis of clutch self-excited vibration in automotive drive line, *SAE Pape*r 951319, 1995.